Table 1
Clinical characteristics of the 12 patients with AML and the 5 patients with normal BM findings

Patient no.	Age	Sex	BM findings	Disease status	Type	Cytogenetics	Blast (%)
1	42	M	AML	Untreated	M2	Normal	87
2	62	M	AML	Relapse	M1	47, XY, del(9)(q13q22),+10	96
3	69	M	AML	Untreated	M4	Normal	90
4	58	M	AML	Untreated	M3	46, XY, t(15;17)	63
5	75	M	AML	Untreated	M4	46, XY, inv(16)	27
6	62	F	AML	Untreated	AML-MRC	NA	24.8
7	72	F	AML	Untreated	AML-MRC	Complex	21
8	42	M	AML	Untreated	M4	46, XY, t(11;17)	25
9	66	M	AML	Untreated	M1	46, XY, t(8;21)	85.4
10	73	F	AML	Untreated	AML-MRC	Complex	44.5
11	65	M	AML	Untreated	AML-MRC	46, XY, t(1;3)	53.3
12	73	M	AML	Untreated	M2	46, XY, add(7)	51.5
13	67	F	Normal			Normal	
14	64	F	Normal			Normal	
15	47	F	Normal			Normal	
16	54	M	Normal			Normal	
17	29	M	Normal			Normal	

Real-time quantitative PCR. Real-time quantitative PCR was carried out on the LightCycler480 system (Roche) using SYBR green reagents according to the manufacturer's instructions. The results were normalized to *Gapdh* levels. Relative expression levels were calculated using the 2-ΔΔCt method (51). The following primers were used for real-time PCR experiments: *Gapdh* forward, TGGCCTCCAAGGAGTAAGAA, and reverse, GGTCTGGGATGGAAATTGTG; *Ncf2* forward, CCAGAAGACCTGGAATTTGTG, and reverse, AAATGCCAACTTTCCCTTTACA; *Tnf* forward, TCTTCTCATTCCTGCTTGTGG, and reverse, GGTCTGGGCCATAGAACTGA; *Il15ra* forward, TAAGCGGAAAGCTGGAACAT, and reverse, TGAGGTCACCTTTGGTGTCA; *Litaf* forward, CTCCAGGACCTTACCAAGCA, and reverse, AGGTGGATTCATTCCCTTCC; *Hoxa9* forward, GGTGCCTGCTGCAGTGTAT, and reverse, GTTCCAGCCAGGAGCGCATAT; *Psma5* forward, CGAGTACGACAGGGGTGTG, and reverse, TGGATGCCAATGGCTGTAG; *Psmd4* forward, GTACATGCGGAACGGAGACT, and reverse, TGTGGTCAGCACCTCACAGT; *Psme3* forward, TTTCAGAGAGCGGATCACAA, and reverse, GGTCATGGATATTTAGAATTGGTTC.

siRNA interference. Specific shRNAs targeting murine *Ikba* mRNA were designed and cloned into pSIREN-RetroQ-ZaGreen vectors. Control shRNA is a nonfunctional construct provided by Clontech. The target sequences, from 5′ to 3′, were: CCGAGACTTTCGAGGAAAT (shIκBα number 1), and AGCTGACCCTGGAAAATCT (shIκBα number. 2).

Immunoblotting. Membranes were probed with the following antibodies: anti-IκBα (Cell Signaling Technology), anti-phospho-IκBα (Ser32) (Cell Signaling Technology), anti-p65 (Santa Cruz Biotechnology Inc.), anti-phospho-p65 (Ser536) (Cell Signaling Technology), anti-β-actin (Cell Signaling Technology), and anti-histone H3 (Cell Signaling Technology). Protein levels were quantified with ImageJ software (NIH). To obtain nuclear and cytoplasmic extracts, an Active Motif Nuclear Extract Kit was used according to the manufacturer's instructions. Cycloheximide treatment assay was performed as described previously, with modification (52). Cells were pretreated with MG132 (20 μM) for 1 hour to initially inhibit the proteasomal degradation of IκBα. Cells were washed twice with medium, then cultured with or without 10 μg/ml of cycloheximide for an additional hour and harvested.

CFC assays. In each experiment, cells were plated onto MethoCult GF M3434 medium (STEMCELL Technologies). Colony numbers in each dish were scored on day 7.

Measurement of TNF-α levels in BM extracellular fluid and conditioned media. BM extracellular fluid was obtained by flushing bilateral femurs and tibia of individual mice with 400 μl PBS. The supernatant was collected after centrifugation. To obtain conditioned media, 0.3–1.0 × 10^6 murine leukemia cells or normal GMPs were cultured in RPMI medium containing 10% FBS and 10 ng/ml IL-3. After a 48-hour incubation, the culture supernatants were collected. The concentration of TNF-α was measured using a murine TNF-α ELISA kit (Gen-Probe Diaclone) according to the manufacturer's instructions. Similarly, 0.5 × 10^4 to 2.0 × 10^4 human AML or normal $CD34^+CD38^-$ cells were cultured for 48 hours in RPMI medium containing 10% FBS and 100 ng/ml SCF, IL-3, and thrombopoietin. The concentration of TNF-α in the harvested supernatants was measured with a human TNF-α Quantikine ELISA kit (R&D Systems).

20S proteasome activity. A 20S proteasome activity assay kit (Cayman Chemical) was used to analyze proteasome activity. A total of 5 × 10^4 freshly isolated normal GMPs, LICs, and non-LICs in each model were assayed according to the manufacturer's protocol. As a control, the proteasome activity of each cell was also assayed after the specific proteasome inhibitor epigallocatechin gallate was added. Fluorescence was measured with a Wallac ARVO V (PerkinElmer), and the proteasome activity of each cell type was calculated by subtracting the respective control value.

Bortezomib treatment studies. For in vivo treatment experiments, LICs of each leukemia model were injected into sublethally irradiated mice: 1 × 10^3 cells in the MLL-ENL or BCR-ABL/NUP98-HOXA9 models, and 1 × 10^4 cells in the MOZ-TIF2 model. Bortezomib was administrated i.p. at doses of 1.0 mg/kg twice weekly for 3 weeks. Treatment was started 1 week after transplantation in the MLL-ENL or BCR-ABL/NUP98-HOXA9 models, and 2 weeks after transplantation in the MOZ-TIF2 model. For experiments analyzing changes in LIC populations, bortezomib was administrated i.p. at doses of 1.0 mg/kg into fully developed leukemic mice. GFP^+ BM cells were collected 24 hours after injection, and surface marker profiles were analyzed.

Analysis of microarray data. We analyzed publicly available gene expression microarray data on murine and human samples from the Gene Expression Omnibus (GEO) database (GEO GSE24797, GSE20377, and GSE24006). A set of CEL files were downloaded from GEO and normalized using the JustRMA function from the Affy package 1.22.1 in Bioconductor. To compare expression profiles of the NF-κB target genes, normalized data were tested for GSEA using previously described NF-κB target gene sets (29), and a nominal *P* value was calculated. For screening of genes with elevated expression levels in LICs compared with those in normal HSPCs, the expression values of individual genes were compared between groups. Genes significantly elevated in LICs from all three leukemia models as determined by an unpaired Student's *t* test ($P < 0.05$)

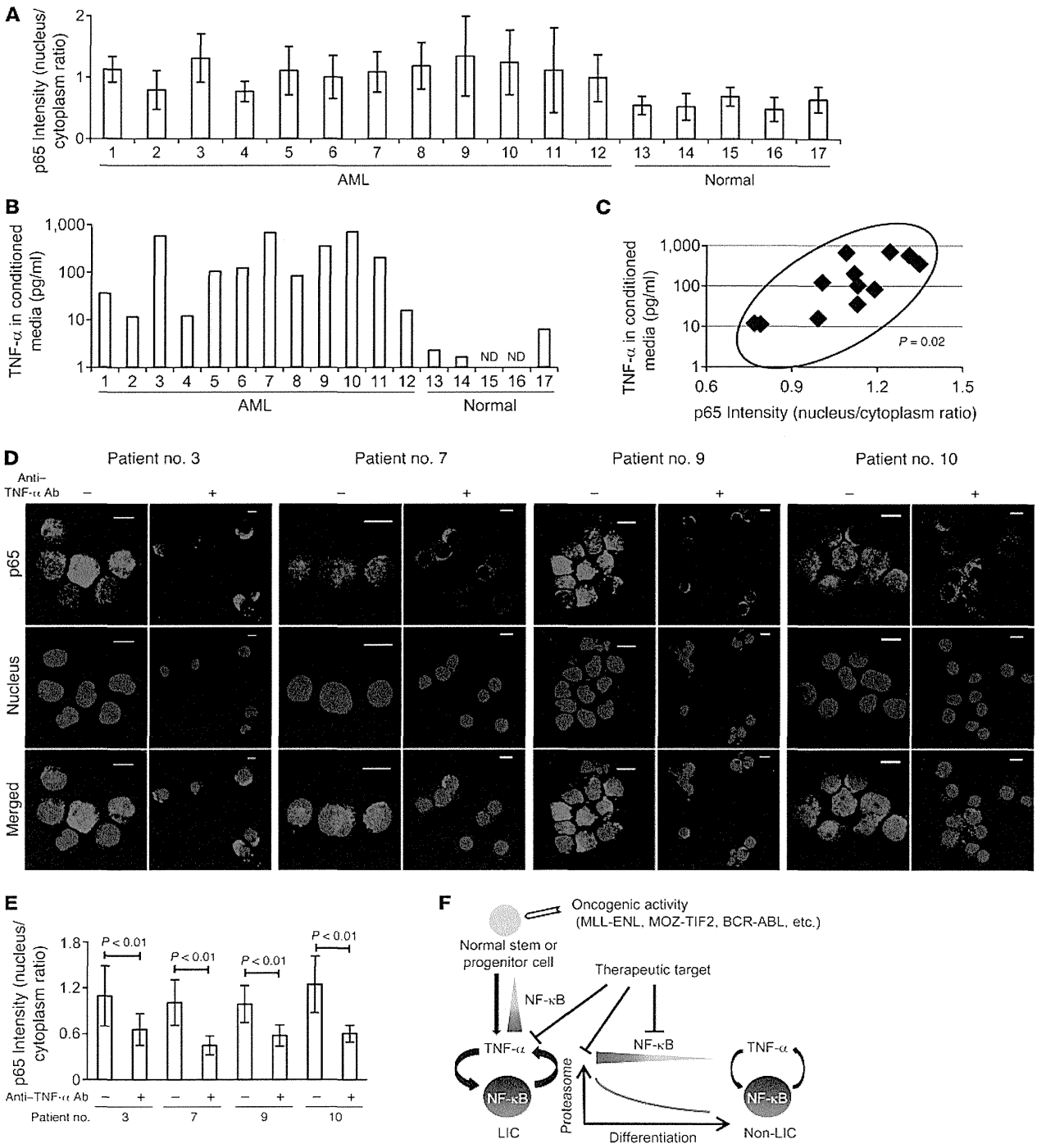

Figure 7

NF-κB/TNF-α positive feedback loop is activated in human AML LICs. (**A**) Quantification of p65 nuclear translocation assessed by the mean nucleus/cytoplasm intensity ratio by immunofluorescence staining. The $CD34^+CD38^-$ fractions isolated from AML or normal BM were analyzed. More than 50 cells were scored in each specimen, and the average intensity ratio with SD is shown. (**B**) TNF-α concentration of culture media conditioned by human AML LICs and normal HSCs measured by ELISA. ND, not detected. (**C**) Correlation between p65 nuclear translocation intensity ratio and TNF-α secretory ability of human AML LICs. (**D**) Immunofluorescence assessment of p65 nuclear translocation in LICs purified from 4 patients after serum-free culture with neutralizing antibody against TNF-α or isotype control. Scale bars: 10 μm. (**E**) Quantification of p65 nuclear translocation of LICs with or without neutralizing antibody against TNF-α assessed by the mean nucleus/cytoplasm intensity ratio. (**F**) Proposed model showing the role of NF-κB signaling in LICs. Positive feedback loop involving NF-κB/TNF-α promotes the maintenance and proliferation of LICs. The signaling is supported by active proteasome machinery, which declines with LIC differentiation.

were selected, among which genes also elevated in human AML LICs (Student's *t* test set at $P < 0.01$) were ultimately selected.

Statistics. Statistical significance of differences between groups was assessed with a 2-tailed unpaired Student's *t* test. Differences were considered statistically significant at a *P* value of less than 0.05. LIC frequency was calculated by Poisson statistics. In leukemia cell transplantation experiments, the overall survival of mice in BM transplantation assays is depicted by a Kaplan-Meier curve. Survival between groups was compared using the log-rank test. To measure the correlation between NF-κB intensity and TNF-α secretion in human AML samples, the Spearman's rank correlation coefficient was used.

Study approval. A total of 12 BM cells derived from patients with AML were obtained from the Department of Hematology and Oncology of the University of Tokyo Hospital. Five BM cells from patients diagnosed with lymphoid neoplasia without BM invasion were used as normal controls. The study was approved by the ethics committee of the University of Tokyo, and written informed consent was obtained from all patients whose samples were collected. All animal experiments were approved by the University of Tokyo Ethics Committee for Animal Experiments.

Acknowledgments

We thank T. Kitamura for the Plat-E packaging cells; H. Nakauchi and M. Onodera for the pGCDNsam-IRES-EGFP retroviral vector; R. Ono and T. Nosaka for the MLL-ENL cDNA; I. Kitabayashi for the MOZ-TIF2 cDNA; W. Hahn for the pBabe-GFP and pBabe-GFP-IκB-SR; and H. Algül and R.M. Schmid for providing the *Rela*-floxed mice. This work was supported by a Grant-in-Aid for Scientific Research A (KAKENHI 12020240) from the Ministry of Education, Culture, Sports, Science and Technology of Japan.

Received for publication December 3, 2012, and accepted in revised form October 17, 2013.

Address correspondence to: Mineo Kurokawa, Department of Hematology and Oncology, Graduate School of Medicine, The University of Tokyo, 7-3-1 Hongo, Bunkyo-ku, Tokyo 113-8655, Japan. Phone: 81.3.5800.9092; Fax: 81.3.5840.8667; E-mail: kurokawa-tky@umin.ac.jp.

1. Bonnet D, Dick JE. Human acute myeloid leukemia is organized as a hierarchy that originates from a primitive hematopoietic cell. *Nat Med.* 1997; 3(7):730–737.
2. Lapidot T, et al. A cell initiating human acute myeloid leukaemia after transplantation into SCID mice. *Nature.* 1994;367(6464):645–648.
3. Ishikawa F, et al. Chemotherapy-resistant human AML stem cells home to and engraft within the bone-marrow endosteal region. *Nat Biotechnol.* 2007; 25(11):1315–1321.
4. Marcucci G, Haferlach T, Döhner H. Molecular genetics of adult acute myeloid leukemia: prognostic and therapeutic implications. *J Clin Oncol.* 2011; 29(5):475–486.
5. Mardis ER, et al. Recurring mutations found by sequencing an acute myeloid leukemia genome. *N Engl J Med.* 2009;361(11):1058–1066.
6. Sen R, Baltimore D. Inducibility of kappa immunoglobulin enhancer-binding protein Nf-κB by a post-translational mechanism. *Cell.* 1986;47(6):921–928.
7. La Rosa FA, Pierce JW, Sonenshein GE. Differential regulation of the c-myc oncogene promoter by the NF-κB rel family of transcription factors. *Mol Cell Biol.* 1994;14(2):1039–1044.
8. Guttridge DC, Albanese C, Reuther JY, Pestell RG, Baldwin AS Jr. NF-κB controls cell growth and differentiation through transcriptional regulation of cyclin D1. *Mol Cell Biol.* 1999;19(8):5785–5799.
9. Duckett CS. Apoptosis and NF-κB: the FADD connection. *J Clin Invest.* 2002;109(5):579–580.
10. Karin M, Greten FR. NF-κB: linking inflammation and immunity to cancer development and progression. *Nat Rev Immunol.* 2005;5(10):749–759.
11. Karin M. Nuclear factor-κB in cancer development and progression. *Nature.* 2006;441(7092):431–436.
12. Pikarsky E, et al. NF-κB functions as a tumour promoter in inflammation-associated cancer. *Nature.* 2004;431(7007):461–466.
13. Guzman ML, et al. Nuclear factor-κB is constitutively activated in primitive human acute myelogenous leukemia cells. *Blood.* 2001;98(8):2301–2307.
14. Guzman ML, et al. Preferential induction of apoptosis for primary human leukemic stem cells. *Proc Natl Acad Sci U S A.* 2002;99(25):16220–16225.
15. Frelin C, et al. Targeting NF-κB activation via pharmacologic inhibition of IKK2-induced apoptosis of human acute myeloid leukemia cells. *Blood.* 2005;105(2):804–811.
16. Carvalho G, et al. Inhibition of NEMO, the regulatory subunit of the IKK complex, induces apoptosis in high-risk myelodysplastic syndrome and acute myeloid leukemia. *Oncogene.* 2007;26(16):2299–2307.
17. Guzman ML, et al. An orally bioavailable parthenolide analog selectively eradicates acute myelogenous leukemia stem and progenitor cells. *Blood.* 2007;110(13):4427–4435.
18. Jenkins C, et al. Nuclear factor-κB as a potential therapeutic target for the novel cytotoxic agent LC-1 in acute myeloid leukaemia. *Br J Haematol.* 2008;143(5):661–671.
19. Jin Y, et al. Antineoplastic mechanism of niclosamide in acute myelogenous leukemia stem cells: inactivation of the NF-κB pathway and generation of reactive oxygen species. *Cancer Res.* 2010;70(6):2516–2527.
20. Takahashi S, et al. Over-expression of Flt3 induces NF-κB pathway and increases the expression of IL-6. *Leuk Res.* 2005;29(8):893–899.
21. Liu S, et al. Sp1/NFκB/HDAC/miR-29b regulatory network in KIT-driven myeloid leukemia. *Cancer Cell.* 2010;17(4):333–347.
22. Nakagawa M, et al. AML1/RUNX1 functions as a cytoplasmic attenuator of NF-κB signaling in the repression of myeloid tumors. *Blood.* 2011; 118(25):6626–6637.
23. Eppert K, et al. Stem cell gene expression programs influence clinical outcome in human leukemia. *Nat Med.* 2011;17(9):1086–1093.
24. Sarry JE, et al. Human acute myelogenous leukemia stem cells are rare and heterogenous when assayed in NOD/SCID/IL2Rγc-deficient mice. *J Clin Invest.* 2011;121(1):384–395.
25. Liu T, et al. Functional characterization of meningioma 1 as collaborating oncogene in acute leukemia. *Leukemia.* 2010;24(3):601–612.
26. Kvinlaug BT, et al. Common and overlapping oncogenic pathways contribute to the evolution of acute myeloid leukemias. *Cancer Res.* 2011; 71(12):4117–4129.
27. Neering SJ, et al. Leukemia stem cells in a genetically defined murine model of blast-crisis CML. *Blood.* 2007;110(7):2578–2585.
28. Wang Y, et al. The Wnt/β-catenin pathway is required for the development ofleukemia stem cells in AML. *Science.* 2010;327(5973):1650–1653.
29. Hinz M, et al. Nuclear factor κB-dependent gene expression profiling of Hodgkin's disease tumor cells, pathogenetic significance, and link to constitutive signal transducer and activator of transcription 5a activity. *J Exp Med.* 2002;196(5):605–617.
30. Gentles AJ, Plevritis SK, Majeti R, Alizadeh AA. Association of a leukemic stem cell gene expression signature with clinical outcomes in acute myeloid leukemia. *JAMA.* 2010;304(24):2706–2715.
31. Kishore N, et al. A selective IKK-2 inhibitor blocks NF-κB-dependent gene expression in interleukin-1 β-stimulated synovial fibroblasts. *J Biol Chem.* 2003;278(35):32861–32871.
32. Algül H, et al. Pancreas-specific RelA/p65 truncation increases susceptibility of acini to inflammation-associated cell death following cerulein pancreatitis. *J Clin Invest.* 2007;117(6):1490–1501.
33. Beg AA, Finco TS, Nantermet PV, Baldwin AS Jr. Tumor necrosis factor and interleukin-1 lead to phosphorylation and loss of IκBα: a mechanism for NF-κB activation. *Mol Cell Biol.* 1993;13(6):3301–3310.
34. DeNardo DG, Coussens LM. Inflammation and breast cancer. Balancing immune response: crosstalk between adaptive and innate immune cells during breast cancer progression. *Breast Cancer Res.* 2007;9(4):212.
35. McLean MH, et al. The inflammatory microenvironment in colorectal neoplasia. *PLoS One.* 2011; 6(1):e15366.
36. Charles KA, et al. The tumor-promoting actions of TNF-α involve TNFR1 and IL-17 in ovarian cancer in mice and humans. *J Clin Invest.* 2009; 119(10):3011–3023.
37. Moore RJ, et al. Mice deficient in tumor necrosis factor-α are resistant to skin carcinogenesis. *Nat Med.* 1999;5(7):828–831.
38. Popivanova BK, et al. Blocking TNF-α in mice reduces colorectal carcinogenesis associated with chronic colitis. *J Clin Invest.* 2008;118(2):560–570.
39. Egberts JH, et al. Anti-tumor necrosis factor therapy inhibits pancreatic tumor growth and metastasis. *Cancer Res.* 2008;68(5):1443–1450.
40. Li J, et al. TNF-α induces leukemic clonal evolution ex vivo in Fanconi anemia group C murine stem cells. *J Clin Invest.* 2007;117(11):3283–3295.
41. Hoang T, Levy B, Ouetto N, Hainan A, Rodriguez-Cimadevilla JC. Tumor necrosis factor α stimulates the growth of the clonogenic cells of acute myeloblastic leukemia in synergy with granulocyte-macrophage colonystimulating factor. *J Exp Med.* 1989;170(1):15–26.
42. Khoury E, et al. Tumor necrosis factor alpha (TNF α) downregulates c-kit proto-oncogene product expression in normal and acute myeloid leukemia $CD34^+$ cells via p55 TNF alpha receptors. *Blood.* 1994;84(8):2506–2514.
43. Zhang B, et al. Altered microenvironmental regulation of leukemic and normal stem cells in chronic myelogenous leukemia. *Cancer Cell.* 2012; 21(4):577–592.
44. Kerbauy DM, Lesnikov V, Abbasi N, Seal S, Scott B, Deeg HJ. NF-κB and FLIP in arsenic trioxide (ATO)-induced apoptosis in myelodysplasticsyndromes (MDSs). *Blood.* 2005;106(12):3917–3925.
45. Adams J. The development of proteasome inhibitors as anticancer drugs. *Cancer Cell.* 2004;5(5):417–421.
46. Chen L, Madura K. Increased proteasome activity,

ubiquitin-conjugating enzymes, and eEF1A translation factor detected in breast cancer tissue. *Cancer Res.* 2005;65(13):5599–5606.
47. Stein SJ, Baldwin AS. Deletion of the NF-κB subunit p65/RelA in the hematopoietic compartment leads to defects in hematopoietic stem cell function. *Blood.* 2013;121(25):5015–5024.
48. Iversen PO, Wiig H. Tumor necrosis factor α and adiponectin in bone marrow interstitial fluid from patients with acute myeloidleukemia inhibit normal hematopoiesis. *Clin Cancer Res.* 2005; 11(19 pt 1):6793–6799.
49. Pronk CJ, Veiby OP, Bryder D, Jacobsen SE. Tumor necrosis factor restricts hematopoietic stem cell activity in mice: involvement of 2 distinct receptors. *J Exp Med.* 2011;208(8):1563–1570.
50. Taniguchi T, Takata M, Ikeda A, Momotani E, Sekikawa K. Failure of germinal center formation and impairment of response to endotoxin in tumor necrosis factor alpha-deficient mice. *Lab Invest.* 1997; 77(6):647–658.
51. Schmittgen TD, Livak KJ. Analyzing real-time PCR data by the Comparative C(T) method. *Nat Protoc.* 2008;3(6):1101–1108.
52. Jain AK, Bloom DA, Jaiswal AK. Nuclear import and export signals in control of Nrf2. *J Biol Chem.* 2005;280(32):29158–29168.

Growth-associated hyperphosphatemia in young recipients accelerates aortic allograft calcification in a rat model

Haruo Yamauchi, MD, PhD,[a] Noboru Motomura, MD, PhD,[a] Ung-il Chung, MD, PhD,[b] Masataka Sata, MD, PhD,[c] Daiya Takai, MD, PhD,[d] Aya Saito, MD, PhD,[a] Minoru Ono, MD, PhD,[a] and Shinichi Takamoto, MD, PhD[a,e]

Objectives: Cardiovascular allografts in the young have limited durability because of early graft calcification. The objective of this study was to examine the hypothesis that growth-associated hyperphosphatemia in youth accelerates aortic allograft calcification by osteogenic transformation of graft medial smooth muscle cells (SMCs).

Methods: The descending aortas of donor rats were subcutaneously transplanted into recipients. Syngeneic (Lewis-to-Lewis) transplantations between 3-week-old "young" (Y) rats and between 10-week-old "adult" (A) rats were combined with standard (ST, 0.9% phosphate) and low-phosphate (LP, 0.2%) diets, resulting in Y-ST, Y-LP, and A-ST groups. Allotransplantations (Brown-Norway–to–Lewis) involving these ages and diets were also made. The grafts and sera were retrieved from recipients after 14 days. Cultured rat aortic SMCs were used to analyze the effects of tumor necrosis factor-alpha (TNF-α) and phosphate on SMC calcification.

Results: In vivo, serum phosphate levels were higher in Y-ST (11.5 mg/dL) than those in Y-LP (8.9 mg/dL) and A-ST (8.5 mg/dL). Graft medial calcification appeared severe only in Y-ST. Allotransplants did not affect these outcomes. Graft medial cells showed phenotypic changes (contractile to synthetic) and osteogenic transformation (α-smooth muscle actin to Runx2 and osteocalcin), together with up-regulated proinflammatory TNF-α and sodium–phosphate cotransporter, Pit-1, despite ages and diets. In vitro, TNF-α induced phenotypic changes and osteogenic transformation of SMCs with Pit-1 up-regulation, but SMC calcification occurred only with high phosphate (4.5 mmol/L).

Conclusions: Growth-associated hyperphosphatemia with inflammatory responses may be essential for accelerating allograft calcification in youth and could be a therapeutic target. (J Thorac Cardiovasc Surg 2013;145:522-30)

ET/BS

Allografts have been useful in cardiovascular surgery for several decades, offering advantages of tissue compatibility, hemodynamics, and avoidance of long-term anticoagulant therapies.[1] However, accelerated graft degeneration and calcification in young patients, especially neonates and infants, limit their durability.[2-5] Immunoreactions may have roles in allograft degeneration,[5] but the etiology of accelerated allograft calcification in young patients is still unidentified.

Vascular calcification has recently been recognized to arise from active osteogenesis.[6] Uremic vasculopathy is characteristic of accelerated medial calcification (Mönckeberg sclerosis), particularly when accompanied with hyperphosphatemia and inflammation.[7] In vitro, inorganic phosphate (Pi) induced vascular smooth muscle cell (SMC) calcification by transforming SMC phenotypes from the myogenic lineage, such as α-smooth muscle actin (α-SMA), to the osteogenic lineage, such as Runx2/Cbfa1 (a transcriptional factor for osteoblastic differentiation) and osteocalcin (noncollagenous bone protein), via type 3 sodium–phosphate cotransporters, Pit-1.[8-10] Tumor necrosis factor-alpha (TNF-α), a proinflammatory cytokine mainly secreted by macrophages, orchestrates inflammatory responses in uremic arteriopathy[11] and also provokes in vitro vascular SMC calcification by osteogenic transformation.[12,13]

Unlike uremia, in which hyperphosphatemia is induced mainly by impaired Pi excretion, growth-associated hyperphosphatemia is characteristic of positive bone turnover in the young inasmuch as growth hormone promotes Pi reabsorption and inhibits the intact parathyroid hormone (iPTH) effect of Pi excretion in the kidney

From the Department of Cardiothoracic Surgery,[a] Division of Tissue Engineering,[b] and Department of Clinical Laboratory,[d] The University of Tokyo Hospital, Tokyo, Japan; the Department of Cardiovascular Medicine,[c] University of Tokushima, Tokushima, Japan; and the Department of Cardiovascular Surgery,[e] Mitsui Memorial Hospital, Tokyo, Japan.

This work was supported by "Kakenhi": Grant-in-Aid for Scientific Research (C: 19591615).

Disclosures: Authors have nothing to disclose with regard to commercial support.

Received for publication Dec 22, 2011; revisions received Feb 9, 2012; accepted for publication March 12, 2012; available ahead of print April 19, 2012.

Address for reprints: Haruo Yamauchi, MD, PhD, 300 Longwood Ave, Boston, MA 02115 (E-mail: hyamauchi-tky@umin.ac.jp).

0022-5223/$36.00

doi:10.1016/j.jtcvs.2012.03.010

Abbreviations and Acronyms

α-SMA	= α-smooth muscle actin
A-allo-ST	= adult allogeneic-transplant with standard diet
A-ST	= adult syngeneic-transplant with standard diet
BN	= Brown-Norway
cAMP/PKA	= cyclic adenosine monophosphate/ protein kinase A
CD	= cluster of differentiation
HP	= high inorganic phosphate
iPTH	= intact parathyroid hormone
LP	= low inorganic phosphate (diet)
PCR	= polymerase chain reaction
Pi	= inorganic phosphate
POD	= postoperative day
RAOSMC	= rat aortic smooth muscle cell
SMC	= smooth muscle cell
ST	= standard (diet)
TNF-α	= tumor necrosis factor-alpha
Y-allo-ST	= young allogeneic-transplant with standard diet
Y-ST	= young syngeneic-transplant with standard diet

tubules.[14] This leads to a higher prevalence of vascular calcification in young uremic patients.[7] In a rat model, the involvement of growth-associated hyperphosphatemia in warfarin-induced arterial calcification was suspected, although its detailed mechanisms were not elucidated.[15] We therefore hypothesize that growth-associated hyperphosphatemia accelerates allograft calcification in young recipients by the osteogenic transformation of graft SMCs in collaboration with the TNF-α–mediated inflammatory response against the grafts. To examine this hypothesis, we used a rat aortic subcutaneous transplant model and a rat aortic SMC (RAOSMC) culture system.

MATERIALS AND METHODS

Animals and Diets

Three-week-old "young" male Lewis rats ($RT1A^lB^l$) and Brown-Norway (BN) rats ($RT1A^nB^n$) weighing 50 to 60 g, 10-week-old "adult" male Lewis (270-290 g) and BN (200-220 g) rats were purchased from Charles River Laboratories Japan (Yokohama, Japan) 1 week before experimentation. A standard (ST) rat diet (0.9% of Pi, 1.1% of calcium) and a low Pi (LP) diet (0.2% Pi, 1.1% calcium) were obtained from Oriental Yeast (Tokyo, Japan).[16]

Rat Aortic Subcutaneous Transplant Model

Rats were anesthetized with intraperitoneal pentobarbital (Nembutal; Hospira, Inc, Lake Forest, Ill; 35 mg/100 g body weight). Under sterile conditions, the descending aortas of the donor rats were harvested and kept in heparinized saline (4°C) as fresh grafts until they were implanted in the subcutaneous pockets of the recipients' abdomens, as described elsewhere.[17] The time from harvest to implantation did not exceed an hour. Each recipient rat received subcutaneous ampicillin (10 mg/100 g body weight) once in its back.

Aortic transplantation was performed between the young rats (the young group) and, separately, between the adult rats (the adult group). Syngeneic (Lewis-to-Lewis) and allogeneic (BN-to-Lewis) transplantations were performed in each age group. Young recipients were fed an ST or an LP diet, whereas adult recipients and all donors received an ST diet throughout the experimental period, resulting in syngeneic- and allogeneic-transplant young (Y-ST and Y-allo-ST) and adult (A-ST and A-allo-ST) groups, all receiving an ST diet, and young groups receiving an LP diet (Y-LP and Y-allo-LP). The young and adult groups before transplantation were defined respectively as the Preop-Y and Preop-A groups. At postoperative day (POD) 7 and POD 14 for the Y-ST group and at POD 14 for the other groups, the recipients were anesthetized as described above, and the grafts were retrieved (n = 6 per group). Then, all recipients were humanely killed by cardiac puncture and the sera were immediately separated by centrifugation. The retrieved grafts and sera were promptly analyzed as follows. Anesthetic and surgical protocols were approved by the Ethics Committee on Animal Research of the University of Tokyo.

Serum Test

The serum calcium, Pi, and iPTH of each rat were measured by the *o*-cresolphthalein complexone method[18] (Calcium C-test; Wako, Osaka, Japan), by the phosphate molybdenum blue method[19] (Phosphor C-test; Wako), and with a rat total iPTH enzyme-linked immunosorbent assay kit (Scantibodies Laboratory, Santee, Calif), respectively. Radioimmunoassays of serum vitamin D [1,25-dihydroxycholecalciferol; $1,25(OH)_2D$] were performed by SRL, Inc (Tokyo, Japan).

Immunohistochemistry, von Kossa Staining, and Electron Microscopy of Grafts

A 4-μm thick frozen section of each graft was examined immunohistochemistry,[20] using primary antibodies against α-SMA (clone 1A4; Sigma-Aldrich, St Louis, Mo), cluster of differentiation 68 (CD68) (AbD Serotec, Oxford, United Kingdom), Runx2 (Sigma-Aldrich), and osteocalcin (Santa Cruz Biotechnology, Santa Cruz, Calif). The positive controls were rat spleen (CD68) and fetal spine (Runx2 and osteocalcin), and the negative control was isotype-matched normal immunoglobulin. Graft calcification was detected by von Kossa staining. Microstructures were observed by transmission electron microscopy (H-7000; Hitachi, Tokyo, Japan) performed as described elsewhere.[21]

Quantification of Calcium and Pi in Grafts

The calcium content of grafts was quantified by atomic absorption spectroscopy[22] by SRL. The tissue Pi content was measured by the Phosphor C-test[19] (Wako). The amounts of calcium and of Pi in each graft were expressed as milligrams per dry weight in grams.

Real-Time Polymerase Chain Reaction (PCR) of Grafts

Total RNA was extracted from each graft tissue and real-time PCR was performed[20] using the following target gene primer sequences: β-actin, (forward) 5′-ATTGAACACGGCATTGTCACC-3′ (reverse) 5′-GCATGAGGGAGCGCGTAAC-3′; α-SMA, (forward) 5′-GAGAAGCTGCTCCAGCTATGT-3′ (reverse) 5′-GATGATGCCGTGTTCTATCG-3′; TNF-α, (forward) 5′-TCCAGAACTCCAGGCGGTGT-3′ (reverse) 5′-GGCAAATCGGCTGACGGTGT-3′; Pit-1, (forward) 5′-GTCTGGTTCTTCGTATGTCCC-3′ (reverse) 5′-GAACTGAACAAGGTTCCCATTA-3′; Runx2, (forward) 5′-ATTCCTCATCCCAGTATGAGAGTAGGT-3′ (reverse)

ET/BS

5′-GCCCAGTGCCCCGTGT-3′; and osteocalcin, (forward) 5′-GAGG GCAGTAAGGTGGTGAATA-3′ (reverse) 5′-AACGGTGGTGCCATA GATG-3′. For osteocalcin determination, betaine monohydrate (Sigma-Aldrich) was added to the PCR solution because of its rich guanine–cytosine content.[23] A duplicate run for each sample was tested and the average was used. The messenger RNA expression of each graft was calculated and expressed as a ratio of that of the internal control, β-actin.

Immunocytochemistry

A cell culture system was prepared as described elsewhere.[8,10] RAOSMCs (Cell Applications, San Diego, Calif) cultured in glass-bottom dishes (Matsunami, Osaka, Japan) were subdivided into a TNF(+) group with 50 ng/mL of TNF-α (Sigma-Aldrich) and a TNF(–) group without it. Mouse osteoblasts (JCRB1178; Health Sciences Foundation, Tokyo, Japan) were cultured without TNF-α. After 7 days, cells were double-stained with α-SMA combined with Runx2, osteocalcin, or normal immunoglobulin, using primary antibodies against α-SMA (clone 1A4, Cy3-conjugated, Sigma-Aldrich), Runx2, and osteocalcin (as described in "Immunohistochemistry"). Each dish with cultured cells was blocked with horse serum and incubated overnight at 4°C with the primary antibodies. Then, the secondary antibodies for Runx2 and osteocalcin labeled with Alexa488 were applied and each dish was observed under a confocal laser scanning microscope (FV300; Olympus, Tokyo, Japan).

Von Kossa Staining and Electron Microscopy of RAOSMCs

RAOSMCs subdivided into TNF(+) and TNF(–) groups as well as mouse osteoblasts were combined with high Pi (HP, 4.5 mmol/l) and low Pi (LP, 1.5 mmol/L) media by adding Pi (NaH_2PO_4/Na_2HPO_4; 0.1 mmol/L, pH 7.0, Wako). After 14 days, cells were fixed and subjected to von Kossa staining.[8] The same groups of RAOSMCs, after 7 days of culture, were fixed, gathered, and centrifuged to form a white pellet, which was treated for transmission electron microscopy.[21]

Calcium Content in RAOSMCs

Pi at 1.5, 2.5, 3.5, and 4.5 mmol/L was administered on RAOSMCs subdivided into TNF(+) and TNF(–) groups. After 14 days, the calcium content of RAOSMCs was determined by the Calcium C-test[18] (Wako) and standardized by their protein content.[8]

Real-time PCR of RAOSMCs

RAOSMCs were divided into 6 groups, to which TNF-α was administered in respective concentrations of 0, 0.1, 1, 10, 50, and 100 ng/mL for 7 days. Then, RNA was extracted with an RNA mini kit (Qiagen, Duesseldorf, Germany), and real-time PCR was performed[20] for β-actin, α-SMA, Runx2, osteocalcin, and Pit-1.

Statistical Analysis

Measurements were presented as mean ± standard error of the mean. Statistical significance was evaluated by analysis of variance, followed by comparisons between control and experimental conditions by the Dunnett test or the Tukey-Kramer honestly significant difference test among multiple groups, using JMP version 9 (SAS Institute, Inc, Cary, NC).

RESULTS

Effects of Young Age, Alloantigen, and Dietary Phosphate Restriction on Graft Calcification

In the young syngeneic- and allogeneic-transplant groups on a standard diet (Y-ST and Y-allo-ST groups), von Kossa staining revealed severe medial calcification, but none in the preoperative young (Preop-Y) and adult (Preop-A) groups, and little or none in the young posttransplant groups on a low phosphate diet (Y-LP and Y-allo-LP) or the adult groups (A-ST and A-allo-ST), irrespective of the presence of alloantigen (Figure 1, *A*). The calcium content of the grafts was significantly higher in the Y-ST and Y-allo-ST groups than in the others (Figure 1, *B*). Similar results were observed in graft Pi content in the syngeneic-transplant groups (Figure 1, *C*). These findings suggest that young age encourages graft calcification regardless of the degree of immunoreaction.

Body Weight and Serum Parameters Relevant to Tissue Calcification

The rats' body weights in the Y-LP and Y-allo-LP groups showed growth retardation. The Y-ST group had, as serum factors relevant to calcium metabolism, higher Pi and lower iPTH levels than the A-ST group, whereas calcium and $1,25(OH)_2D$ were not significantly different. In the Y-LP group, Pi and iPTH were significantly lower and calcium and $1,25(OH)_2D$ higher than in the Y-ST group. Similar differences owing to age factors and dietary Pi inhibition were observed in the allogeneic group, although calcium and $1,25(OH)_2D$ tended to be higher than in the syngeneic group (Table 1). These results suggest that only the serum Pi level reflects the severity of graft calcification.

Microstructures of the Graft Medial Cells

To investigate why young age encourages graft calcification, we further examined syngeneic grafts of both age groups. On electron microscopy, the graft medial cells in both age groups appeared flat preoperatively, with cytoplasms rich in actin filaments, typical characteristics of the contractile phenotype of SMCs (Figure 2, *A* and *B*). The intracellular actin filaments appeared diminished in size and number, but were still present at POD 7 (Figure 2, *C*), although further diminished in both age groups at POD 14 (Figure 2, *D* and *E*). Postoperatively, however, matrix vesicles, characteristic of the synthetic phenotype of SMCs, appeared in the cytoplasm, and matrices were partially secreted into the extracellular spaces in both groups. Dense calcium deposition was observed in the Y-ST group (Figure 2, *C* and *E*), whereas the margins of matrices were only slightly calcified in the A-ST group (Figure 2, *D*). In the Y-LP group, as in the Y-ST group, matrix vesicles were present, but without calcified matrices (Figure 2, *F*).

Gene Expressions of the Graft Media

Immunohistochemical staining showed that the graft media preoperatively expressed abundant α-SMA, but no CD68, Runx2, or osteocalcin in either age group. Postoperatively, α-SMA was much less expressed in the grafts,

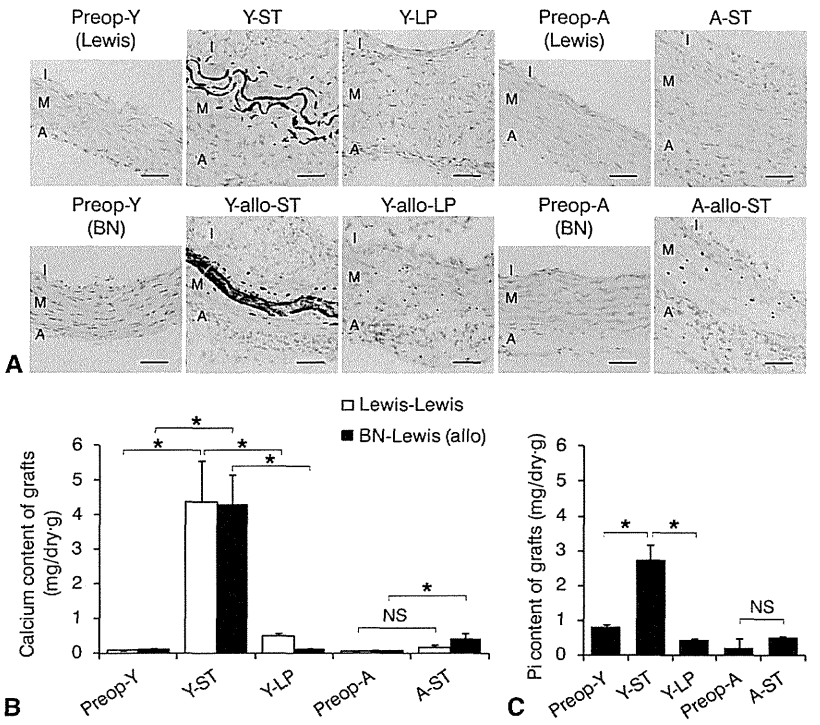

FIGURE 1. Analyses of aortic graft calcification. A, Von Kossa staining of the grafts showing calcification in black. *Preop-Y* and *Preop-A,* Preoperative young and adult groups; *Y-ST* and *Y-allo-ST,* young syngeneic- and allogeneic-transplant groups at postoperative day *(POD)* 14 on a standard *(ST)* diet, respectively; *Y-LP* and *Y-allo-LP,* young syngeneic- and allogeneic-transplant groups, respectively, on a low phosphate *(LP)* diet; *A-ST* and *A-allo-ST,* syngeneic- and allogeneic-transplant adult groups on an ST diet, respectively. *BN,* Brown-Norway; *I,* intima; *M,* media; *A,* adventitia. Magnification ×200. *Bar* = 100 μm. B and C, Calcium and inorganic phosphate *(Pi)* contents of grafts (n = 6 per group). *$P < .05$ by Tukey-Kramer honestly significant difference test; *NS,* not significant.

whereas CD68-positive macrophages appeared in and around the graft media. Runx2 and osteocalcin were also stained along the elastic graft media laminae (Figure 3, *A*). In real-time PCR, mRNA expression of α-SMA was down-regulated, whereas those of TNF-α, Pit-1, Runx2, and osteocalcin were up-regulated in the postoperative Y-ST, Y-LP, and A-ST groups. However, there were no significant differences among the Y-ST, the Y-LP, and the A-ST groups, except that Runx2 was significantly higher in the A-ST than in the Y-ST group (Figure 3, *B-F*).

Coeffects of TNF-α and Phosphate on Rat Aortic SMCs

The role of SMCs in graft calcification was examined using the RAOSMC culture. First, we investigated the effects of TNF-α on RAOSMCs. Immunocytochemistry

TABLE 1. Body weight and serum parameters of rat aortic transplant models

	Body weight (g)	Calcium (mg/dL)	Pi (mg/dL)	1,25(OH)$_2$D (pg/mL)	iPTH (pg/mL)
Preop-Y	55.0 ± 1.7*	8.7 ± 0.4*	10.2 ± 0.6	274.2 ± 18.2	201.1 ± 25.8
Y-ST	117.7 ± 2.5	10.9 ± 0.2	11.5 ± 0.6	346.5 ± 10.6	264.3 ± 15.5
Y-LP	89.0 ± 2.5*	13.6 ± 0.8*	8.9 ± 0.4*	846.2 ± 83.8*	69.4 ± 10.6*
Y-allo-ST	125.7 ± 1.6	12.7 ± 0.1	10.5 ± 0.4	465.3 ± 17.2	Not examined
Y-allo-LP	99.7 ± 2.9*	16.2 ± 0.4*	8.9 ± 0.7*	971.0 ± 20.1*	Not examined
Preop-A	281.3 ± 3.3*,†	10.0 ± 0.3	8.1 ± 0.3*	237.0 ± 30.7	385.4 ± 36.0†
A-ST	304.7 ± 1.6*	11.0 ± 0.2	8.5 ± 0.3*	251.0 ± 24.7	721.6 ± 84.2*
A-allo-ST	322.7 ± 2.9*,†	15.5 ± 1.2*,†	8.5 ± 0.3*	389.7 ± 20.1†	Not examined

The data represent mean ± standard error (n = 6 per group). *Pi,* Inorganic phosphate; *1,25(OH)$_2$D,* 1,25-dihydroxycholecalciferol; *iPTH,* intact parathyroid hormone; *Preop-Y,* young group before transplantation; *Y-ST,* young syngeneic-transplant with standard diet; *Y-LP,* young syngeneic-transplant with low inorganic phosphate diet; *Y-allo-ST,* young allogeneic-transplant with standard diet; *Y-allo-LP,* young allogeneic-transplant with low inorganic phosphate diet; *Preop-A,* adult group before transplantation; *A-ST,* adult syngeneic-transplant with standard diet; *A-allo-ST,* adult allogeneic-transplant with standard diet. *$P < .05$ vs Y-ST in both age groups. †$P < .05$ vs A-ST in the adult group by the Dunnett method.

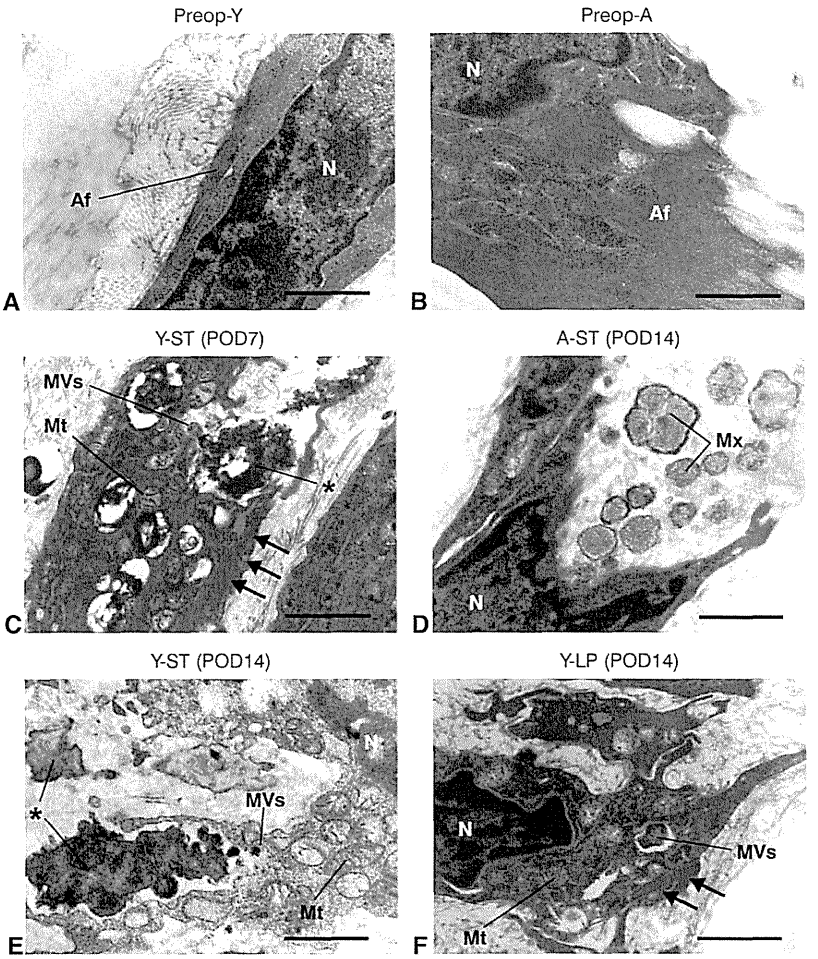

FIGURE 2. Microstructures of the grafts (electron microscopy). The photographs of the grafts were obtained preoperatively (A and B) and at POD 7 from the Y-ST group (C) and at POD 14 from the A-ST, Y-ST, and Y-LP groups (D to F). *Arrows* indicate actin filaments. *Asterisks* indicate calcium deposition. *POD,* Postoperative day; *Y-ST,* young syngeneic-transplant with standard diet; *A-ST,* adult syngeneic-transplant with standard diet; *Y-LP,* young syngeneic-transplant with low inorganic phosphate diet; *N,* nucleus; *Af,* actin filaments; *Mt,* mitochondria; *MVs,* matrix vesicles; *Mx,* matrix. Magnification ×20,000. *Bar* = 1 μm. For abbreviations see Figure 1.

showed that RAOSMC protein expression had shifted from myogenic (α-SMA) to osteogenic (Runx2 and osteocalcin) on TNF-α treatment (50 ng/mL) (Figure 4, *A*). Using real-time PCR, the mRNA expression of α-SMA in RAOSMCs was significantly down-regulated, whereas those of Runx2, osteocalcin, and Pit-1 were up-regulated by TNF-α, both dose-dependently (Figure 4, *B* and *C*). Second, we evaluated the coeffects of TNF-α and Pi on RAOSMCs. RAOSMCs were severely calcified on costimulation with TNF-α (50 ng/mL) and high Pi (4.5 mmol/L), but not with either alone (Figure 4, *D*). In RAOSMCs, calcium content increased significantly in proportion to the Pi concentration only in the TNF-α-treated media (50 ng/mL) (Figure 4, *E*). Electron microscopy revealed diminished numbers of actin filaments in RAOSMCs with TNF-α, but newly developed rough endoplasmic reticula and matrix vesicles, despite the Pi concentration in the TNF-α-treated media. Calcium deposition in the matrix vesicles appeared only in RAOSMCs treated with high Pi media (Figure 4, *F*).

DISCUSSION

In this study, our transplant models demonstrated that aortic allograft calcification, accelerated in young, but not adult, rats, was suppressed by lowering serum Pi to the adult level, suggesting that growth-associated hyperphosphatemia promotes allograft calcification. Not only serum Pi but also calcium, $1,25(OH)_2D$, and iPTH have been reported to promote vascular calcification.[7] In the present study, however, the levels of calcium and $1,25(OH)_2D$ were similar in the 2 age groups, and both rose on Pi suppression. Thus, these factors cannot be the primary causes

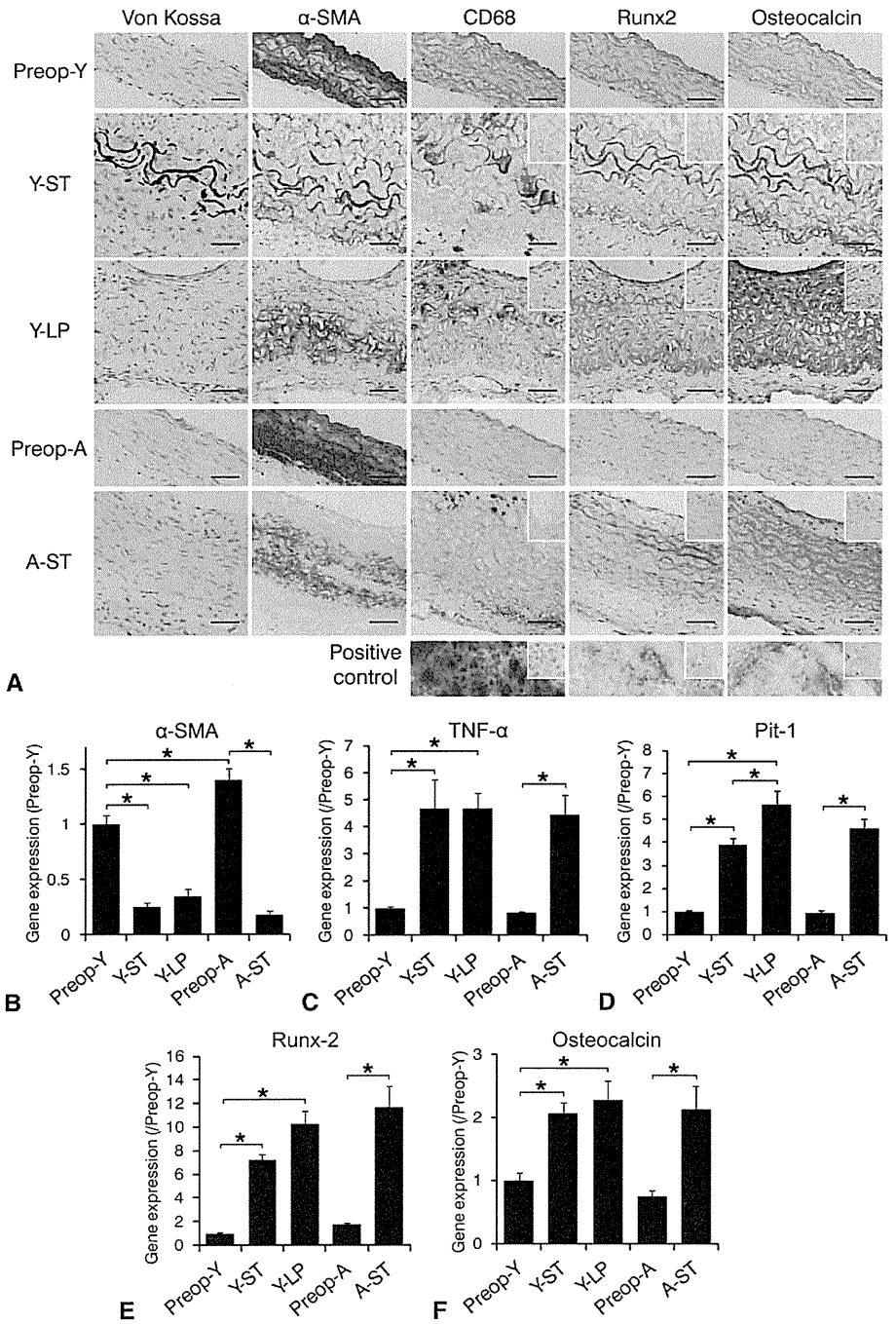

FIGURE 3. Gene expressions in the grafts. A, Von Kossa staining and immunohistochemical stainings of smooth muscle cell-alpha *(α-SMA),* cluster of differentiation *(CD)* 68, Runx2, and osteocalcin in the same specimens of syngeneic-transplant group grafts. Protein expression appears *red* on immunostaining. *Positive control*: Rat spleen for CD68; rat fetal spine for Runx2 and osteocalcin. *Small window*: Staining of normal immunoglobulin. Magnification ×200. *Bar* = 100 μm. B-F, Real-time polymerase chain reaction *(PCR)* analyses of α-SMA, TNF-α, Pit-1, Runx2, and osteocalcin in the grafts. Each gene expression is shown as a ratio of that of the Preop-Y group (n = 6 per group). *$P < .05$ by Tukey-Kramer honestly significant difference test. For abbreviations see Figures 1 and 2. *CD,* Cluster of differentiation; *TNF-α,* tumor necrosis factor-alpha; *Pit-1,* sodium–phosphate cotransporter; *Preop-Y,* young group before transplantation; *Y-ST,* young syngeneic-transplant with standard diet; *Y-LP,* young syngeneic-transplant with low inorganic phosphate diet; *A-ST,* adult syngeneic-transplant with standard diet; *Preop-A,* adult group before transplantation.

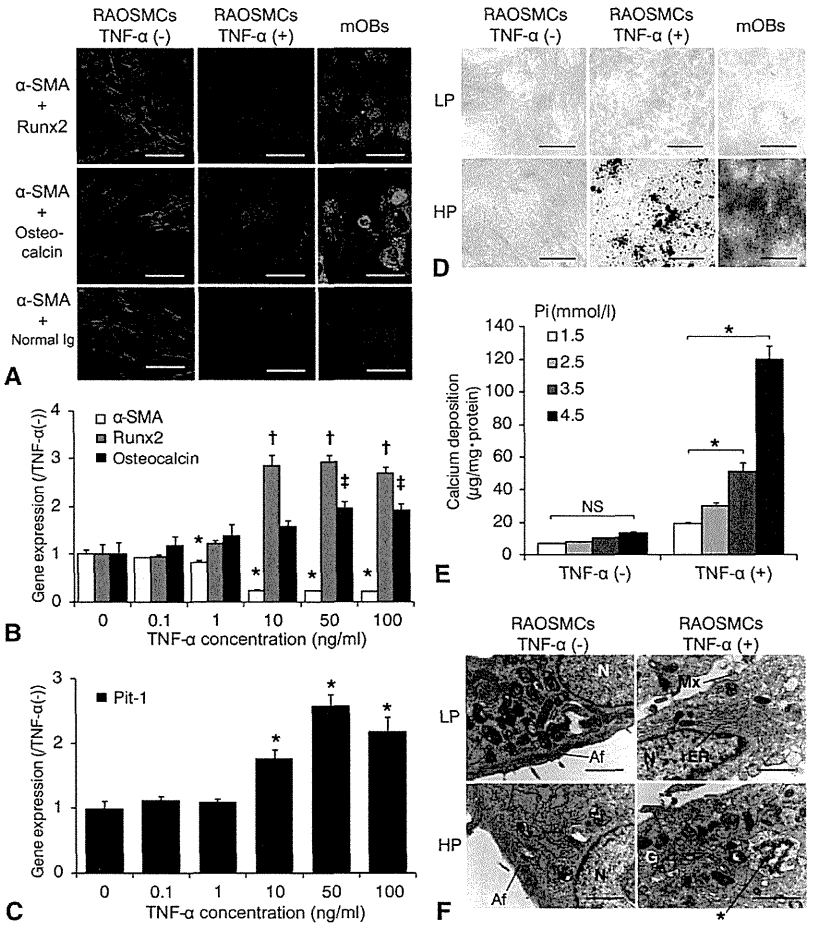

FIGURE 4. Effects of TNF-α and Pi on SMCs. A, Immunocytochemistry of α-SMA, Runx2, and osteocalcin proteins in the cultured rat aortic SMCs *(RAOSMCs)* and mouse osteoblast-like cells *(mOBs;* positive control). α-SMA antibody was conjugated with Cy3 *(red)*. Runx2 and osteocalcin antibodies as well as normal immunoglobulin *(Ig,* negative control) were labeled with Alexa488 *(green)*. Nuclei were counterstained with 4′,6-diamidino-2-phenylindole *(DAPI; blue)*. TNF-α(+), 50 ng/mL of TNF-α in the media. Magnification ×400. *Bar* = 50 μm. B and C, Real-time PCR analyses of α-SMA, Runx2, osteocalcin, and Pit-1. Each gene expression is shown as a ratio of that without TNF-α (0 ng/mL) (n = 4 per group). *,†,‡P < .05 compared with 0 ng/mL of TNF-α using the Dunnett test. D, Calcium deposition is highlighted in *black* by von Kossa staining. *HP* and *LP,* high phosphate (4.5 mmol/L) and low phosphate (1.5 mmol/L) in the media. Magnification ×100. *Bar* = 200 μm. E, Quantified calcium deposition in the RAOSMCs cultured with 1.5 to 4.5 mmol/L of Pi. *P < .0001 by the Dunnett test (n = 4 per group). F, RAOSMCs stimulated by TNF-α (50 ng/mL), HP, or both, analyzed by electron microscopy. *Asterisk* indicates calcium deposition. *G,* Golgi apparatus. Magnifications: the TNF-α-HP group, ×25,000; others, ×20,000. *Bar* = 1 μm. For abbreviations see Figures 1 to 3. *TNF-α,* Tumor necrosis factor-alpha; *Pi,* inorganic phosphate; *SMC,* smooth muscle cell; *α-SMA,* α-smooth muscle actin; *RAOSMC,* rat aortic smooth muscle cell; *PCR,* polymerase chain reaction. Same as described in the abbreviation box and in the legend of Figure 3.

ET/BS

of graft calcification observed only in the young. The presence of lower iPTH levels in the young than in adults, presumably owing to the effects of growth hormone,[14] is inconsistent with the hyperparathyroidemia-related ectopic calcification observed in uremia.[7]

Regarding the role of Pi on vascular calcification, in vitro studies reported that high Pi enhanced the Pit-1 expression together with Pi transport and triggered osteogenic transformation of SMCs.[8,10] However, in the present study, why were the grafts in young animals calcified only after transplantation? And why were osteogenic changes observed in all posttransplant group grafts? Our response to this is to suspect the effects of inflammation in posttransplant grafts. TNF-α expression in posttransplant grafts was enhanced together with the osteogenic markers and Pit-1, irrespective of the animals' ages or diets (Figure 3, *C-F*). Similar findings are reported in a recent study showing that the aortas of uremic patients, independently of calcification status, enhanced coexpression of TNF-α and bone morphogenetic protein-2,[11] which is

a potent regulator of osteoblastic differentiation,[24] and the expression of the latter was enhanced similarly in the posttransplant grafts in both age groups in our study (data not shown). In vitro, TNF-α acts on vascular calcification through the cyclic adenosine monophosphate/protein kinase A (cAMP/PKA) pathway by enhancing DNA binding of Runx2/Cbfa1 and activating downstream factors, for example, osteocalcin and osteopontin.[12] More recently, Pi transport via Pit-1 was reported to be a necessary mediator of mineralization downstream from the cAMP/PKA pathway triggered by TNF-α, although Pit-1 expression was not enhanced by the cAMP/PKA inducer.[25] This is inconsistent with our present finding of enhanced Pit-1 concurrent with TNF-α expression in the posttransplant grafts and cultured SMCs, which indicates involvement of a signaling pathway other than cAMP/PKA. Then, our cultured SMCs showing marked calcification only when both TNF-α and high Pi were given were consistent with our transplant model showing significant calcification only in posttransplant grafts in young recipients. These observations suggest that a low Pi diet or Pi binders may prevent allograft calcification in young patients. Considering the limited growth rates observed in the rats fed a low-Pi diet, however, local Pi inhibition or systemic Pi suppression to the threshold level, which can reduce the graft calcification without accompanying growth disturbance, may be necessary.

Study Limitations

A subcutaneous transplant model using weanling rats has conventionally been used to explore the mechanisms and preventive methods of tissue calcification.[17,22] The pattern of graft media calcification seen in the allografts after orthotopic implantation resembled that in the present study.[26] The suggested mechanisms of accelerating graft calcification, however, require validation in circulatory implant models, inasmuch as factors such as blood contact and pulsatile pressure may affect allograft calcification differently. Despite the definite roles of Pi, the influences of other relevant factors on allograft calcification and degeneration, such as immunoreactions, apoptosis, and the function of pyrophosphate, need further investigation. Also, this study has not examined whether the growth retardation was related to the suppression of musculoskeletal development or other hormonal dysfunctions. Further investigation is necessary to clarify the mechanism of this growth retardation and to develop therapeutic strategies with weaker adverse effects.

CONCLUSIONS

In summary, this rat model suggests that growth-associated hyperphosphatemia in young recipients, in conjunction with osteogenic transformation of graft medial SMCs, may be critical in promoting vascular allograft calcification and is therefore potentially a therapeutic target for inhibiting allograft calcification and improving graft durability in young recipients.

We are grateful to Mr Satoru Fukuda for technical advice regarding electron microscopy and to Mr C. W. P. Reynolds for his careful linguistic assistance with this manuscript.

References

1. Fontan F, Choussat A, Deville C, Doutremepuich C, Coupilland J, Vosa C. Aortic valve homografts in the surgical treatment of complex cardiac malformations. *J Thorac Cardiovasc Surg*. 1984;87:649-57.
2. Clarke DR, Campbell DN, Hayward AR, Bishop DA. Degeneration of aortic valve allografts in young recipients. *J Thorac Cardiovasc Surg*. 1993;105: 934-41.
3. Tweddell JS, Pelech AN, Frommelt PC, Mussatto KA, Wyman JD, Fedderly RT, et al. Factors affecting longevity of homograft valves used in right ventricular outflow tract reconstruction for congenital heart disease. *Circulation*. 2000; 102(Suppl III):III130-5.
4. Yankar AC, Alexi-Meskhishvili V, Weng Y, Schorn K, Lange PE, Hetzer R. Accelerated degeneration of allografts in the first two years of life. *Ann Thorac Surg*. 1995;60(Suppl):S71-6.
5. Shaddy RE, Hawkins JA. Immunology and failure of valved allografts in children. *Ann Thorac Surg*. 2002;74:1271-5.
6. Vattikuti R, Towler DA. Osteogenic regulation of vascular calcification: an early perspective. *Am J Physiol Endocrinol Metab*. 2004;286:E686-96.
7. Querfeld U. The clinical significance of vascular calcification in young patients with end-stage renal disease. *Pediatr Nephrol*. 2004;19:478-84.
8. Jono S, McKee MD, Murry CE, Shioi A, Nishizawa Y, Mori K, et al. Phosphate regulation of vascular smooth muscle cell calcification. *Circ Res*. 2000;87: E10-7.
9. Steitz SA, Speer MY, Curinga G, Yang HY, Haynes P, Aebersold R, et al. Smooth muscle cell phenotypic transition associated with calcification: upregulation of Cbfa1 and downregulation of smooth muscle lineage markers. *Circ Res*. 2001; 89:1147-54.
10. Li X, Yang HY, Giachelli CM. Role of the sodium-dependent phosphate cotransporter, Pit-1, in vascular smooth muscle cell calcification. *Circ Res*. 2006;98: 905-12.
11. Koleganova N, Piecha G, Ritz E, Schirmacher P, Müller A, Meyer HP, et al. Arterial calcification in patients with chronic kidney disease. *Nephrol Dial Transplant*. 2009;24:2488-96.
12. Tintut Y, Patel J, Parhami F, Demer LL. Tumor necrosis factor-alpha promotes in vitro calcification of vascular cells via the cAMP pathway. *Circulation*. 2000;102:2636-42.
13. Shioi A, Katagi M, Okuno Y, Mori K, Jono S, Koyama H, et al. Induction of bone-type alkaline phosphatase in human vascular smooth muscle cells: roles of tumor necrosis factor-alpha and oncostatin M derived from macrophages. *Circ Res*. 2002;91:9-16.
14. Woda CB, Halaihel N, Wilson PV, Haramati A, Levi M, Mulroney SE. Regulation of renal NaPi-2 expression and tubular phosphate reabsorption by growth hormone in the juvenile rat. *Am J Physiol Renal Physiol*. 2004;287: F117-23.
15. Price PA, Faus SA, Williamson MK. Warfarin-induced artery calcification is accelerated by growth and vitamin D. *Arterioscler Thromb Vasc Biol*. 2000;20: 317-27.
16. Subcommittee on Laboratory Animal Nutrition, Committee on Animal Nutrition, Board on Agriculture, National Research Council. Nutrient Requirements of the Laboratory Rat. In: Subcommittee on Laboratory Animal Nutrition, National Research Council, editor. Nutrient requirements of laboratory animals. 4th revised ed. Washington (DC): The National Academies Press; 1995. p. 27-8.
17. Webb CL, Nguyen NM, Schoen FJ, Levy RJ. Calcification of allograft aortic wall in a rat subdermal model. Pathophysiology and inhibition by Al^{3+} and aminodiphosphonate preincubations. *Am J Pathol*. 1992;141:487-96.
18. Moorehead WR, Biggs HG. 2-Amino-2-methyl-1-propanol as the alkalizing agent in an improved continuous-flow cresolphthalein complexone procedure for calcium in serum. *Clin Chem*. 1974;20:1458-60.
19. Drewes PA. Direct colorimetric determination of phosphorus in serum and urine. *Clin Chim Acta*. 1972;39:81-8.
20. Saito A, Motomura N, Kakimi K, Narui K, Noguchi N, Sasatsu M, et al. Vascular allografts are resistant to methicillin-resistant *Staphylococcus aureus* through

ET/BS

indoleamine 2,3-dioxygenase in a murine model. *J Thorac Cardiovasc Surg.* 2008;136:159-67.
21. Sata M, Tanaka K, Ishizaka N, Hirata Y, Nagai R. Absence of p53 leads to accelerated neointimal hyperplasia after vascular injury. *Arterioscler Thromb Vasc Biol.* 2003;23:1548-52.
22. Brockbank KG, Song YC. Mechanisms of bioprosthetic heart valve calcification. *Transplantation.* 2003;75:1133-5.
23. Henke W, Herdel K, Jung K, Schnorr D, Loening SA. Betaine improves the PCR amplification of GC-rich DNA sequences. *Nucleic Acids Res.* 1997;25:3957-8.
24. Hruska KA, Mathew S, Saab G. Bone morphogenetic proteins in vascular calcification. *Circ Res.* 2005;97:105-14.
25. Huang MS, Sage AP, Lu J, Demer LL, Tintut Y. Phosphate and pyrophosphate mediate PKA-induced vascular cell calcification. *Biochem Biophys Res Commun.* 2008;374:553-8.
26. Flameng W, Jashari R, De Visscher G, Mesure L, Meuris B. Calcification of allograft and stentless xenograft valves for right ventricular outflow tract reconstruction: an experimental study in adolescent sheep. *J Thorac Cardiovasc Surg.* 2011;141:1513-21.

TEB-2013-0578-ver9-Kagami_1P
Type: review-article

TISSUE ENGINEERING: Part B
Volume 00, Number 00, 2014

DOI: 10.1089/ten.teb.2013.0578

The Use of Bone Marrow Stromal Cells (Bone Marrow-Derived Multipotent Mesenchymal Stromal Cells) for Alveolar Bone Tissue Engineering: Basic Science to Clinical Translation

Hideaki Kagami, DDS, PhD,[1–3] Hideki Agata, DDS, PhD,[4] Minoru Inoue, DDS, PhD,[1,2] Izumi Asahina, DDS, PhD,[4] Arinobu Tojo, MD, PhD,[1] Naohide Yamashita, MD, PhD,[2] and Kozo Imai, MD, PhD[5]

Bone tissue engineering is a promising field of regenerative medicine in which cultured cells, scaffolds, and osteogenic inductive signals are used to regenerate bone. Human bone marrow stromal cells (BMSCs) are the most commonly used cell source for bone tissue engineering. Although it is known that cell culture and induction protocols significantly affect the *in vivo* bone forming ability of BMSCs, the responsible factors of clinical outcome are poorly understood. The results from recent studies using human BMSCs have shown that factors such as passage number and length of osteogenic induction significantly affect ectopic bone formation, although such differences hardly affected the alkaline phosphatase activity or gene expression of osteogenic markers. Application of basic fibroblast growth factor helped to maintain the *in vivo* osteogenic ability of BMSCs. Importantly, responsiveness of those factors should be tested under clinical circumstances to improve the bone tissue engineering further. In this review, clinical application of bone tissue engineering was reviewed with putative underlying mechanisms.

Introduction

ATROPHIC ALVEOLAR BONE is one of the major obstacles for dental implant therapy and there are a large number of patients without sufficient bone volume. For patients with severe bone atrophy, autologous bone grafts have been performed.[1] However, even the amount of harvesting bone is small and the procedure is accompanied by swelling and pain of the donor site.[2] Although bioartificial bone substitutes have been frequently used, the ability to induce bone regeneration is limited.[3] Accordingly, less invasive and more efficient bone regeneration therapy is awaited, such as tissue engineering.

The first results of clinical bone tissue engineering were published in 2001.[4] In this study, the regeneration of long bone defects was tested using hydroxyapatite blocks together with cultured autologous bone marrow stromal cells (BMSCs). This tissue engineering-based approach proved the feasibility of this concept. The results from a preliminary clinical study of alveolar bone regeneration were published thereafter.[5] In this review, studies on clinical alveolar bone tissue engineering are summarized. Then, the problems associated with current tissue engineering were also discussed.

Bone Tissue Engineering and Stem Cells

Cells are considered as a major component of tissue engineering. Although the role of transplanted cells during bone tissue regeneration is still controversial, it has been proved that the transplanted cells could survive, proliferate, and differentiate into osteogenic phenotype.[6] There is accumulating evidence that the level and quality of regeneration is affected by the ability of transplanted cells.[7] Accordingly, it is important to establish an optimal cell culture protocol to maximize the function of osteogenic cells. Surprisingly, the BMSC ability to differentiate into osteoblast-like cells is easily diminished during passage and no bone formation was observed after several passages (Fig. 1).[7,8] Furthermore, cell seeding density and the period of induction also affect *in vivo* osteogenic ability. It has been

[1]Tissue Engineering Research Group, Division of Molecular Therapy, The Advanced Clinical Research Center, The Institute of Medical Science, The University of Tokyo, Tokyo, Japan.
[2]Department of Advanced Medical Science, Clinic for Bone Regeneration, IMSUT Hospital, The Institute of Medical Science, The University of Tokyo, Tokyo, Japan.
[3]Department of Oral and Maxillofacial Surgery, Matsumoto Dental University Dental School, Shiojiri, Japan.
[4]Unit of Translational Medicine, Department of Regenerative Oral Surgery, Nagasaki University Graduate School of Biomedical Sciences, Nagasaki, Japan.
[5]Center for Antibody and Vaccine, IMSUT Hospital, The Institute of Medical Science, The University of Tokyo, Tokyo, Japan.

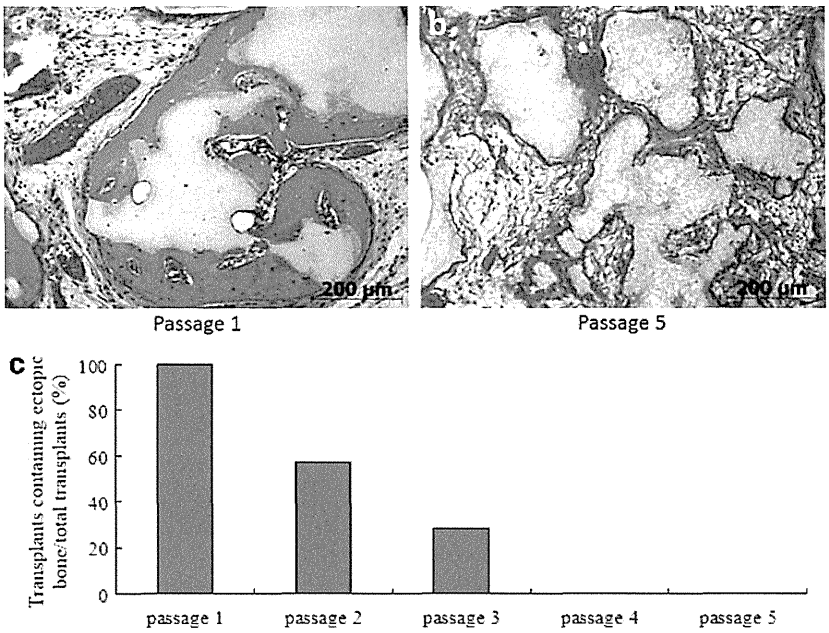

FIG. 1. Effect of passage number on ectopic *in vivo* osteogenic ability. Upper panels showing ectopic bone formation at the back of nude mice with tissue-engineered bone using passage 1 (**a**) and passage 5 (**b**) human bone marrow stromal cells (BMSCs). The success of ectopic bone formation quickly decrease after passage and no bone formation was observed after passage 4 (**c**). Note that the ability is quickly lost during passage. Modified from Agata *et al.*[7] Color images available online at www.liebert pub.com/teb

shown that basic fibroblast growth factor (bFGF) is beneficial to maintain *in vivo* osteogenic ability of BMSCs.[7]

Clinical Studies on Alveolar Bone Tissue Engineering

The results from clinical studies on alveolar bone tissue engineering using BMSCs were first reported in 2004. In this study, bone marrow-derived MSCs were mixed with platelet-rich plasma as a scaffold.[8] Bone regeneration was observed in all cases. Another clinical study utilized BMSCs and hydroxyapatite granules. BMSCs were induced into osteogenic cells for 1 week and transplanted. In this study, bone formation was observed in three cases, but there was no apparent bone formation from the transplanted cells in

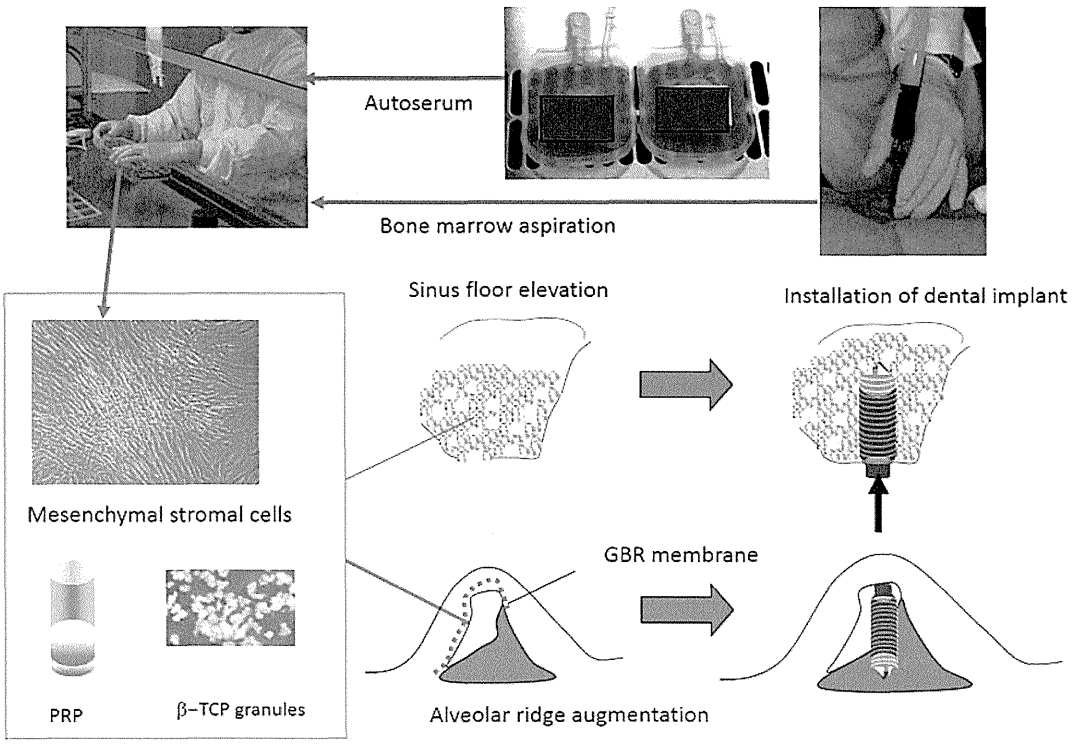

FIG. 2. The procedure for clinical study of alveolar bone regeneration at The Research Hospital, The Institute of Medical Science, The University of Tokyo. β-TCP; PRP. Color images available online at www.liebertpub.com/teb

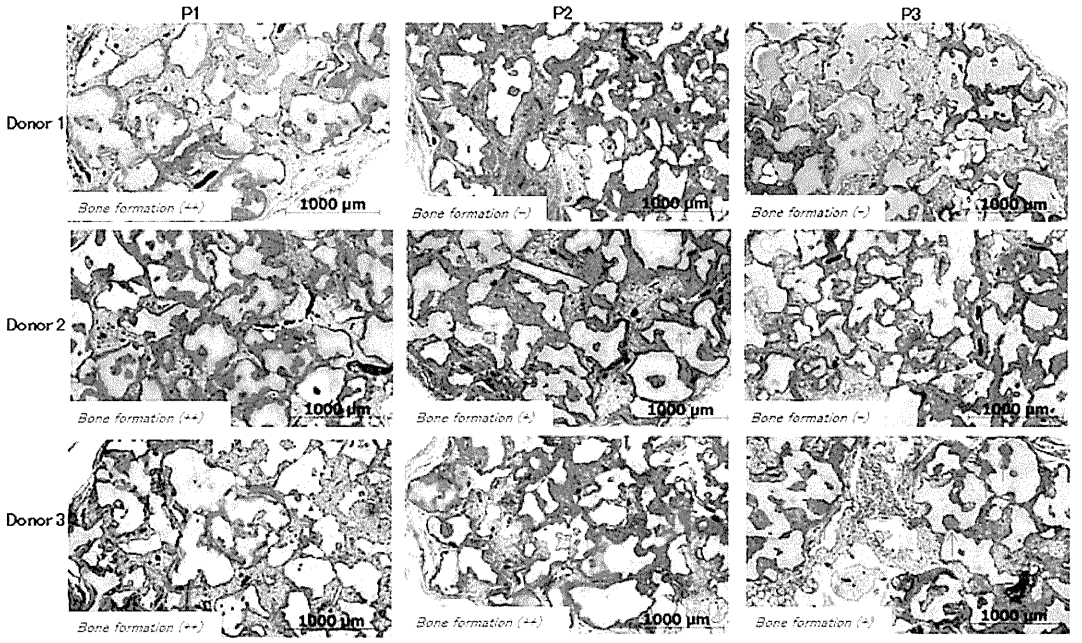

FIG. 3. Individual (donor) variations of *in vivo* osteogenic ability and their changes during passage. Note that the effect of passage differed between individuals. Color images available online at www.liebertpub.com/teb

cases where the atrophy was severe. Thus, the efficacy of clinical alveolar bone tissue engineering for severe atrophy cases remains controversial.

We have conducted a clinical study of bone tissue engineering for severe atrophy of alveolar bone. In this study, autologous BMSCs were transplanted together with platelet-rich plasma gel and β-TCP granules as scaffolds (Fig. 2). The results from a 2-year observation showed that bone regeneration was observed in all patients, although significant individual variations in cell growth, differentiation, and levels of bone regeneration were observed (Asahina *et al.*, manuscript in preparation). This type of study, focused on severe atrophy cases, may prove the usefulness of alveolar bone tissue engineering. In terms of safety, no side effects or related complications have been reported, which may imply the relatively safety nature of alveolar bone tissue engineering using BMSCs.

Toward the Establishment of Reliable Alveolar Bone Tissue Engineering Using BMSCs

Although clinical studies have confirmed the feasibility and safety of alveolar bone tissue engineering using BMSCs, one of the important clinical benchmarks is the efficacy for severe atrophy cases. The results from focused studies with selected cases will provide the evidence. Another important problem is the individual variation as shown by basic and preliminary clinical studies. Since the shape and the size of bone defect vary among individuals, it might be impossible to completely eliminate such variations. Accordingly, it should be important to minimize the variation in other factors, such as cells. In terms for BMSCs, there was no significant difference in the expression of mesenchymal stem cell markers during passage.[7] In contrast, a large variation was observed in the *in vivo* bone forming ability among donors and during passage.[7,8] We believe the usage of early passage cells as well as growth factors (bFGF) may minimize the variation, which should be tested under clinical settings.

In spite of the number of studies and the clinical efficacy of bone tissue engineering, it is not a standard treatment at present. It is necessary to show the superiority of clinical outcome compared with standard autologous bone transplantation and allogenic (or xenogenic) transplantation. Furthermore, tissue engineering requires special facility for cell culture and there is a requirement for many safety examinations, which may also increase the cost for treatment. Those technologies, which may support the widespread use of bone tissue engineering, should be investigated.

Tissue engineering is one of the most rapidly progressing fields and alveolar bone is still an attractive target for tissue engineering.[9] The application of bone tissue engineering is not limited for dental implants and is successfully applied for other diseases such as nonunion fractures[10] and alveolar clefts.[11,12]

Disclosure Statement

No competing financial interests exist.

References

1. Jensen, S.S., and Terheyden, H. Bone augmentation procedures in localized defects in the alveolar ridge: clinical results with different bone grafts and bone-substitute materials. Int J Oral Maxillofac Implants **24 Suppl,** 218, 2009.
2. Clavero, J., and Lundgren, S. Ramus or chin grafts for maxillary sinus inlay and local onlay augmentation: comparison of donor site morbidity and complications. Clin Implant Dent Relat Res **5,** 154, 2003.

3. Becker, W., Urist, M., Becker, B.E., Jackson, W., Parry, D.A., Bartold, M., Vincenzzi, G., De Georges, D., and Niederwanger, M. Clinical and histologic observations of sites implanted with intraoral autologous bone grafts or allografts. 15 human case reports. J Periodontol **67,** 1025, 1996.
4. Quatro, R., Mastrogiacomo, M., and Cancedda, R. Repair of large bone defects with the use of autologous bone marrow stromal cells. N Engl J Med **344,** 385, 2001.
5. Yamada, Y., Ueda, M., Hibi, H., and Nagasaka, T. Translational research for injectable tissue-engineered bone regeneration using mesenchymal stem cells and platelet-rich plasma: from basic research to clinical case study. Cell Transplant **13,** 343, 2004.
6. Meijer, G.J., de Bruijn, J.D., Koole, R., and van Blitterswijk, C.A. Cell based bone tissue engineering in jaw defects. Biomaterials **29,** 3053, 2008.
7. Agata, H., Asahina, I., Watanabe, N., Ishii, Y., Kubo, N., Ohshima, S., Yamazaki, M., Tojo, A., and Kagami, H. Characteristic change and loss of *in vivo* osteogenic abilities of human bone marrow stromal cells during passage. Tissue Eng Part A **16,** 663, 2010.
8. Sugiura, F., Kitoh, H., and Ishiguro, N. Osteogenic potential of rat mesenchymal stem cells after several passages. Biochem Biophys Res Commun **316,** 233, 2004.
9. Egusa, H., Sonoyama, W., Nishimura, M., Atsuta, I., and Akiyama, K. Stem cells in dentistry—Part II: clinical applications. J Prosthodont Res **56,** 229, 2012.
10. Shoji, T., Ii, M., Mifune, Y., Matsumoto, T., Kawamoto, A., Kwon, S.M., Kuroda, T., Kuroda, R., Kurosaka, M., and Asahara, T. Local transplantation of human multipotent adipose-derived stem cells accelerates fracture healing via enhanced osteogenesis and angiogenesis. Lab Invest **90,** 637, 2010.
11. Pradel, W., and Lauer, G. Tissue-engineered bone grafts for osteoplasty in patients with cleft alveolus. Ann Anat **194,** 545, 2012.
12. Janssen, N.G., Weijs, W.L., Koole, R., Rosenberg, A.J., and Meijer, G.J. Tissue engineering strategies for alveolar cleft reconstruction: a systematic review of the literature. Clin Oral Investig **18,** 219, 2014.

Address correspondence to:
Hideaki Kagami, DDS, PhD
Tissue Engineering Research Group
Division of Molecular Therapy
The Advanced Clinical Research Center
The Institute of Medical Science
The University of Tokyo
4-6-1 Shirokanedai
Minato-ku
Tokyo 108-8639
Japan

E-mail: kagami@ims.u-tokyo.ac.jp

Received: September 15, 2013
Accepted: January 30, 2014
Online Publication Date:

TISSUE ENGINEERING: Part A
Volume 20, Numbers 7 and 8, 2014

DOI: 10.1089/ten.tea.2013.0333

Original Article

Stage-Specific Embryonic Antigen 4 in Wharton's Jelly–Derived Mesenchymal Stem Cells Is Not a Marker for Proliferation and Multipotency

Haiping He, MD,[1–3] Tokiko Nagamura-Inoue, MD, PhD,[2] Hajime Tsunoda, MD, PhD,[4] Miki Yuzawa, MT,[2] Yuki Yamamoto, MT,[2] Pariko Yorozu, BNS,[2] Hideki Agata, PhD,[5] and Arinobu Tojo, MD, PhD[1,2]

Background: Umbilical cord Wharton's jelly (WJ) is a rich source of mesenchymal stem cells (MSCs) similar to bone marrow (BM) and adipose tissues. Stage-specific embryonic antigen (SSEA)4 has been reported as a stem cell marker in BM-derived MSCs, but whether $SSEA4^+$ cells have growth and differentiation advantages over $SSEA4^-$ cells remains controversial. To gain insight into the role of SSEA4, we studied $SSEA4^+$ cells in WJ-derived MSCs (WJ-MSCs).
Methods: WJ-MSCs were collected by the explant (WJe-MSCs) or collagenase methods (WJc-MSCs) and analyzed by flow cytometry and reverse-transcription polymerase chain reaction (RT-PCR). To evaluate whether culture conditions influenced the SSEA4 expression, WJe-MSCs were cultured in the medium supplemented with different fetal bovine serum (FBS) concentrations.
Results: SSEA4 was expressed for a long-term culture. In contrast, $SSEA3^+$ disappeared rapidly in early passages of the culture. The incidence of $SSEA4^+$ and $SSEA3^+$ cells was similar between WJe-MSCs and WJc-MSCs at passages P0–P9, except for transient depletion of SSEA4 expression in early passages of WJe-MSCs. These were $CD73^+CD105^+$ cells that express embryonic stem cell markers detected by RT-PCR. No differences in growth and differentiation ability of osteocytes and adipocytes were observed between the sorted $SSEA4^+$ cells and $SSEA4^-$ cells. Further, SSEA4 expression in WJe-MSCs was significantly correlated with FBS concentration in the culture medium.
Discussion: SSEA4, which may display altered expression profiles in response to culture conditions, may not be an essential marker of WJ-MSC multipotency.

Introduction

Umbilical cord (UC) Wharton's jelly (WJ) is a rich source of mesenchymal stem cells (MSCs) along with bone marrow (BM) and adipose tissue.[1–3] WJ-derived MSCs (WJ-MSCs) exhibit the characteristics of MSCs as defined by the International Society for Cellular Therapy (ISCT) criteria. First, MSCs are plastic adherent when maintained in standard culture conditions; second, they are positive for CD105, CD73, HLA-class I, and CD90 and negative for CD45 and HLA-DR surface molecules; and third, MSCs have the pluripotent ability of various mesoderm lineages to generate adipocytes, osteoblasts, and chondrocytes.[4,5] Similar to BM-derived MSCs (BM-MSCs), WJ-MSCs have the potential to differentiate into mesoderm-derived tissues, endoderm, and ectoderm lineages, such as endothelial cells, cardiac myoblasts, pancreatic cells, hepatocytes, and neurogenic cells.[6,7] Hsieh *et al.* compared the gene expression profiles of BM-MSCs and WJ-MSCs and reported that WJ-MSCs were more primitive and more similar to embryonic stem (ES) cells than BM-MSCs.[8,9] On the basis of this data, we isolated the primitive MSCs in WJ-MSCs that are similar to ES cells. Markers of pluripotent, undifferentiated ES cells express several nuclear transcription factors, such as *Oct4, Nanog*, and *SOX2*, and cell surface antigens that have been used to define ES cells, including stage-specific embryonic antigen (SSEA)3 and

[1]Division of Molecular of Therapy, Center for Advanced Medical Research, The Institute of Medical Science, The University of Tokyo, Tokyo, Japan.
[2]Department of Cell Processing and Transfusion, The Institute of Medical Science, The University of Tokyo, Tokyo, Japan.
[3]Department of Hematology, First People Hospital of Yunnan Province, Kunming, China.
[4]Department of Obstetrics, NTT Medical Center Tokyo Hospital, Tokyo, Japan.
[5]Tissue Engineering Research Group, Division of Molecular Therapy, The Institute of Medical Science, The University of Tokyo, Tokyo, Japan.

4. The latter two cell surface antigens are present on human ES cells and human embryonic carcinoma cells and are downregulated as these cells differentiate. SSEA3 and SSEA4 are epitopes on the related glycosphingolipids (GSLs), GL-5 and GL-7, respectively. GSLs consist of a carbohydrate moiety or a chain linked to ceramide[10] and appear to be attractive surface markers for sorting live ES-like primitive cells from WJ-MSCs. However, the role of SSEA3 and SSEA4 as pluripotent markers remains controversial, with different laboratories reporting variable results. Gang *et al.* reported that SSEA4 is a marker for BM-MSCs,[11] and Wakao *et al.* showed that SSEA3 is a pluripotent stem cell marker on MSCs defined as multilineage-differentiating stress-enduring (Muse) cells.[12,13] In contrast, Brimble *et al.* demonstrated that both SSEA3 and SSEA4 are not essential for human ES cell pluripotency, as proven by GSL inhibitors.[14]

To obtain $SSEA3^+/4^+$-rich MSCs, we compared the following two major collection methods from the UC: the explant method (WJe-MSCs) and the collagenase-treatment method (WJc-MSCs). We previously reported that WJe-MSCs by the explant method were preferred over that by the collagenase method because WJ-MSCs treated with collagenase sometimes showed decreased cell viability due to the lytic activity of collagenases. However, we could not determine whether the cells migrating from the tissue in the explant method could be selected and induced to differentiate to some degree.

In this study, we compared SSEA3/4 expression in WJ-MSCs collected by different methods. To examine the potential role of SSEA4 in WJ-MSCs, we studied the growth and differentiation ability of cells sorted by SSEA4 expression and factors that influence its expression.

Materials and Methods

Isolation and culture of adherent cells

The present study was approved by the Ethics Committee of the Institute of Medical Science, University of Tokyo, Japan, and the NTT Medical Center Tokyo hospital. Informed consent was obtained from mothers planning to have cesarean sections. UCs were collected aseptically from full-term cesarean section patients after informed consent. The UCs were transferred after collection and the process was initiated within 24 h of delivery. The UC surface was rinsed with phosphate-buffered saline (PBS; Gibco–BRL) containing antibiotics and antifungal reagents Anti–Anti (Antibiotic–Antimycotic, 100×; Gibco–BRL). After removing two arteries and one vein, the remaining WJ tissues were minced into 1–2 mm^3 fragments and divided into two groups for the explant and collagenase-treatment methods (Fig. 1A). In the explant method, the minced fragments were aligned and attached at regular intervals in 10-cm culture dishes. After the fragments were semi-dried and firmly attached to the bottom, the culture medium was gently poured into the dishes.[1,15] In the collagenase-treatment group, the minced WJ tissues were incubated in 1 mg/mL collagenase type I solution (Sigma–Aldrich) in α-MEM (Gibco–BRL) with shaking at 37°C for 2–3 h.[15,16] The cells were then washed with α-MEM supplemented with 10% fetal bovine serum (FBS) and seeded in 10-cm tissue culture dishes with the culture medium as described earlier.[1] The culture medium was refreshed once a week for 3–4 weeks until fibroblast-like adherent cells reached 80–90% confluence. The first-harvested master cells were defined as passage 0 (P0; Fig. 1B). The adherent cells and tissue fragments (Fig. 1A) were rinsed once with PBS and detached using 10% trypsin solution (TrypLE Express; Invitrogen) followed

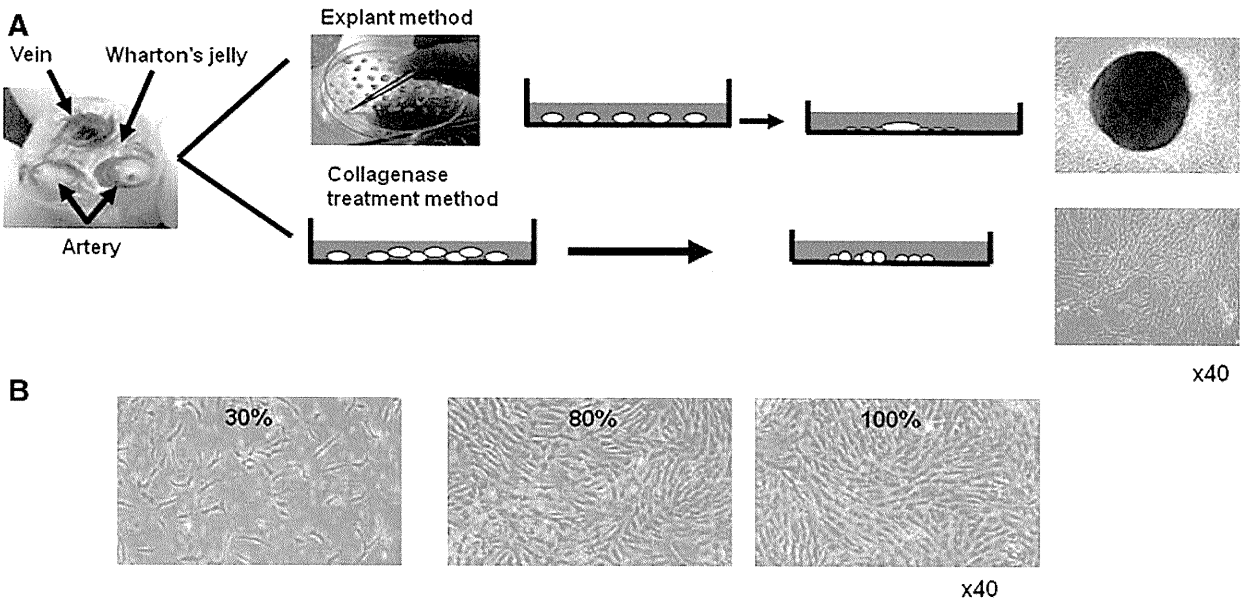

FIG. 1. Umbilical cord Wharton's jelly–derived mesenchymal stem cells (WJ-MSCs). **(A)** MSCs were collected from umbilical cord WJ tissue by the explant method (WJe-MSCs) and by the collagenase-treatment method (WJc-MSCs). Photographs of migrating cells from the minced tissue in the explant method and adherent cells from the scattered cells in the collagenase-treatment method are shown. **(B)** Both WJe-MSCs and WJc-MSCs were spindle-shaped fibroblast-like cells. Color images available online at www.liebertpub.com/tea

by washing with α-MEM supplemented with 10% FBS. In the explant method, the cells and tissue fragments were filtered to remove the tissue fragments. The harvested cells, other than those undergoing further analysis, were immediately cryopreserved in 10% DMSO/5% dextran 40 solution. For serial cultures, the cells were inoculated at 2×10^5 cells per 10-cm-diameter dish and counted at each passage.

Flow cytometry analysis and sorting

Standard flow cytometry (FCM) techniques were used to determine the typical cell surface markers of WJ-MSCs. WJ-MSCs were stained with the following mouse monoclonal antibodies (mAbs): phycoerythrin (PE)–conjugated anti-human CD73 (BD), CD271 (Miltenyi), and HLA-ABC (BD); fluorescein isothiocyanate (FITC)–conjugated anti-human CD90 (BD), CD105 (eBioscience), HLA-DR (BD), and CD45 (BD), FITC-, PE-, and Alexa Fluor–conjugated anti-mouse IgGs (BD) were used as isotypic controls. Dead cells were identified by staining with propidium iodide. To detect the ES cell markers in WJ-MSCs, Alexa Fluor–conjugated mouse anti-human SSEA4 (Clone MC813-70; BD) and FITC-conjugated rat anti-human SSEA3 (Clone MC631; BD) together with the MSC markers CD73 or CD105 mAbs were used. The stained cells were acquired with an FACSCaliber (BD) and analyzed by FlowJo (Tomy Digital Biology, Co. Ltd.). For cell sorting, WJe-MSCs were stained with Alexa-conjugated anti-human SSEA4 and PE-conjugated anti-human CD73 antibodies. The cells were acquired with an FACSAria cell sorting system (BD) and sorted by SSEA4, SSEA3, and CD73 expression.

Proliferation assays of sorted SSEA4$^+$ and SSEA4$^-$ MSCs

To evaluate the proliferative abilities of sorted SSEA4$^+$ and SSEA4$^-$ WJe-MSCs, the sorted cells were plated at 1×10^4/well in six-well plates (Greiner Bio-one) and cultured in α-MEM supplemented with 10% FBS. The cells were harvested every week and the cell numbers were counted with trypan blue (Gibco–BRL) for 9 weeks.

SSEA4 expression in WJ-MSCs with different FBS concentrations

To evaluate whether culture conditions influenced the SSEA4 expression, WJe-MSCs (P0) were cultured at 1×10^5 cells/well in six-well plates ($n=3$) in α-MEM with the indicated FBS concentrations. After 1 week, the SSEA4, SSEA3, and CD73 expression was analyzed by FCM. To study the influence of the proliferation of WJe-MSCs on SSEA4 expression, we explored the time-course experiment to see the relationship between SSEA4 expression and WJe-MSC growth curve. WJe-MSCs were plated in six-well plates with indicated concentrations of FBS, and the cell number was counted to figure the growth curve on indicated days. The cells were analyzed by FCM to analyze the expression of SSEA3, SSEA4, and CD73.

Further, to analyze the influence of FBS on SSEA4$^-$ WJe-MSCs, SSEA4$^+$ and SSEA4$^-$ WJe-MSCs were cultured in 12-well plates with different concentrations of FBS followed by FCM.

SSEA4 expression in BM-MSCs with different FBS concentrations

To clarify that the phenomena of SSEA4 expression are limited to the WJe-MSCs, we studied the SSEA4 expression in BM-MSCs obtained from BM mononuclear cells (MNCs). Frozen BM-MNCs were purchased from Lonza Walkersville, Inc. BM-MNCs (8×10^5/well) were seeded in six-well plates and grown at 37°C with 5% CO_2. On days 0–21, the proportion of CD45-, SSEA4-, and CD73-positive or -negative cells were analyzed by FCM. To see the influence of FBS on BM-MSCs, we continued to culture BM-MNCs in α-MEM supplemented with 10% FBS and obtained the MSCs. BM-MSCs at p2 were plated in six-well plates to figure the growth curve and analyzed the incidence of CD45, SSEA3, SSEA4, and CD73 by FCM, as described in WJe-MSCs.

RNA isolation and reverse-transcription polymerase chain reaction analysis

Total RNAs were extracted from WJ-MSCs at P3 and from sorted SSEA4$^+$ and SSEA4$^-$ MSCs using TRIzol® Reagent (Invitrogen Corp.). Reverse-transcription polymerase chain reaction (RT-PCR) was performed using the PrimeScript RT-PCR Kit (Takara Shuzou) according to the manufacturer's instructions. The ES markers *Nanog*, *Oct4*, *Klf4*, and *Sox2*[17] and *glyceraldehyde-3-phosphate dehydrogenase* (GAPDH) as the control were amplified from the synthesized cDNAs by PCR with the primer pairs shown in Table 1. The amplification conditions were 35 cycles of denaturation at 94°C for 30 s, annealing at 56°C for 30 s, and

TABLE 1. HUMAN PRIMER SEQUENCES USED FOR REVERSE-TRANSCRIPTION POLYMERASE CHAIN REACTION

Gene	*Accession*		*Primer sequence*	*Product size (bp)*
hOCT3/4	NM-002701	Sense	5′ GACAGGGGGAGGGGAGGAGCTAGG 3′	144
		Anti-sense	5′ CTTCCCTCCAACCAGTTGCCCCAAAC 3′	
REX1	NM-174900	Sense	5′ CAGATCCTAAACAGCTCGCAGAAT 3′	306
		Anti-sense	5′ GCGTACGCAAATTAAAGTCCAGA 3′	
NANOG	NM-024865	Sense	5′ CAGCCCCGATTCTTCCACCAGTCCC 3′	391
		Anti-sense	5′ CGGAAGATTCCCAGTCGGGTTCACC 3′	
hSOX2	NM-003106	Sense	5′ GGGAAATGGGAGGGGTGCAAAAGAGG 3′	151
		Anti-sense	5′ TTGCGTGAGTGTGGATGGGATTGGTG 3′	
hKLF4	NM-004235	Sense	5′ ACGATCGTGGCCCCGGAAAAGGACC 3′	397
		Anti-sense	5′ TGATTGTAGTGCTTTCTGGCTGGGCTCC 3′	
hGAPDH	NM-002046	Sense	5′ AACAGCCTCAAGATCATCAGC 3′	338
		Anti-sense	5′ TTGGCAGGTTTTTCTAGACGG 3′	